Accepted Manuscript

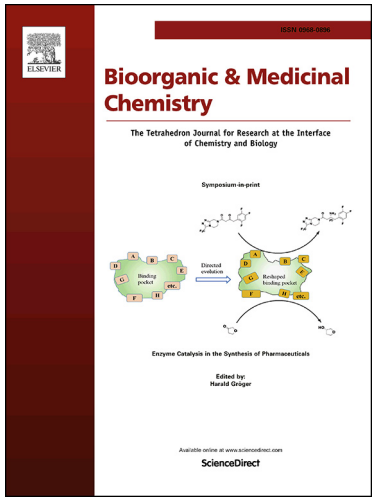

Design, synthesis, molecular modelling and *in vitro* cytotoxicity analysis of novel carbamate derivatives as inhibitors of Monoacylglycerol lipase

Simone Lauria, Cristiana Perrotta, Silvana Casati, Ilaria Di Renzo, Roberta Ottria, Ivano Eberini, Luca Palazzolo, Chiara Parravicini, Pierangela Ciuffreda

PII: S0968-0896(17)32482-3
DOI: https://doi.org/10.1016/j.bmc.2018.04.024
Reference: BMC 14307

To appear in: *Bioorganic & Medicinal Chemistry*

Received Date: 22 December 2017
Revised Date: 27 March 2018
Accepted Date: 10 April 2018

Please cite this article as: Lauria, S., Perrotta, C., Casati, S., Renzo, I.D., Ottria, R., Eberini, I., Palazzolo, L., Parravicini, C., Ciuffreda, P., Design, synthesis, molecular modelling and *in vitro* cytotoxicity analysis of novel carbamate derivatives as inhibitors of Monoacylglycerol lipase, *Bioorganic & Medicinal Chemistry* (2018), doi: https://doi.org/10.1016/j.bmc.2018.04.024

Design, synthesis, molecular modelling and *in vitro* cytotoxicity analysis of novel carbamate derivatives as inhibitors of Monoacylglycerol lipase

Simone Lauria[a], Cristiana Perrotta[a], Silvana Casati[a], Ilaria Di Renzo[a], Roberta Ottria[a], Ivano Eberini[b], Luca Palazzolo[b], Chiara Parravicini[b], Pierangela Ciuffreda[a*]

[a] *Dipartimento di Scienze Biomediche e Cliniche "Luigi Sacco", Università degli Studi di Milano, Italy*
[b]*Dipartimento di Scienze Farmacologiche e Biomolecolari, Università degli Studi di Milano, Italy*

*Corresponding author:
Pierangela Ciuffreda
Università degli Studi di Milano-Dipartimento di Scienze Biomediche e Cliniche "Luigi Sacco"
Via G.B. Grassi 74, 20157 Milano, Italy
Tel: ++39-02-50319695
e-mail: pierangela.ciuffreda@unimi.it

Abstract

Monoacylglycerol lipase (MAGL) has an essential role in the catabolic pathway of the endocannabinoid 2-arachidonoylglycerol, which makes it a potential target for highly specific inhibitors for the treatment of a number of diseases. We designed and synthesized a series of carbamate analogues of URB602. We evaluated their inhibitory activity toward human MAGL *in vitro* both in cell culture and lysates. The target compounds exhibited moderate to excellent inhibitory activity against MAGL. The most promising compound **2b** showed good inhibitory activity with IC_{50} value of 4.5 ± 0.70 μM reducing MAGL activity to 82% of controls at 10 μM compared to 66% for the parent compound URB602. Interestingly, compounds **2b** and **2c** induce cell death through the inhibition of MAGL. Molecular modelling approaches and docking studies, used to investigate inhibitory profiles, indicated that trifluoromethyl substitutions of the aryl group and the benzene ring present at the oxygen side of the carbamate molecule had a significant impact on the activity.

Keywords: Monoacylglycerol lipase, carbamate, structure-activity relationships, cytotoxicity, anti-proliferative

1. Introduction

Monoacylglycerol lipase (MAGL) is a soluble serine hydrolase that peripherally associates with cell membranes and was originally isolated from adipose tissues where it catalyzes the final step in lipolysis, thereby liberating free fatty acids and glycerol for fuel or lipid synthesis.[1] The enzyme is found both in the brain (cortex, hippocampus, cerebellum, thalamus, striatum) and in peripheral tissues such as the kidney, ovary, testis, adrenal gland, adipose tissue and heart.[2] 2-arachidonoylglycerol (2-AG), the main substrate of MAGL,[3,4] is an endocannabinoid that activates cannabinoid (CB) receptors CB1 and CB2. The principal route for 2-AG inactivation is via enzymatic hydrolysis generating arachidonic acid and glycerol. MAGL is the first hydrolase implicated in 2-AG degradation, responsible for approximately 85% of 2-AG hydrolysis.[5]

The involvement of endocannabinoids (ECs) in a wide range of physiological and pathological processes, including anxiety, pain, feeding, cognition, food intake, inflammation, memory, and emotions,[6,7] has focused on the development of MAGL inhibitors for their therapeutic potential as new analgesics and anxiolytics.[8–10] Furthermore, studies using both non-selective and highly selective MAGL inhibitors and MAGL knockout mice have found that MAGL is the conjunction between ECs and prostaglandin signaling networks being the

primary source of arachidonic acid for the production of pro-inflammatory eicosanoids in the nervous system, in the liver, and in the lungs.[11] Blocking the activity of this enzyme by specific inhibitors[12] or genetic knock-out[13] increases local levels of ECs leading to lesser side effect potential compared to global CB receptor activation.[14] Moreover genetic as well as pharmacological inactivation of MAGL in mice causes a strong increase of monoglycerides in many tissues including brain, liver, adipose tissue, intestine, and others, demonstrating a major role of the enzyme in monoglyceride catabolism.[3,4,7]

MAGL inhibitors have been shown to have anti-cancer properties not only through modulating the endocannabinoid eicosanoid network, but also by controlling fatty acid release for the synthesis of protumorigenic signaling lipids.[15] The therapeutic potential of MAGL inhibitors, the fact that this enzyme is well characterized and its crystal structure has been reported,[16] have pointed out MAGL as target for several studies. Several classes of MAGL inhibitors have been identified from early reversible ones, such as URB602,[17] to carbamoylating agents that react with the catalytic serine, such as JZL184.[18] Over the last few years, MAGL inhibitors with novel structures have been developed such as JJKK-048 lead MAGL inhibitor from piperidine triazole urea class.[19]

The work presented here has focused on synthesis, structure-activity relationship (SAR), and biological evaluation of novel carbamate derivatives, potentially targeting MAGL. These derivatives were obtained on the basis of structural modifications of the parent compound URB602. URB602 is a suitable scaffold for designing MAGL inhibitors since it increases levels of 2-AG without altering levels of *N*–arachidonoylethanolamide (anandamide, AEA) in both *in vitro* and *in vivo* models[20] and does not affect the levels of other lipid metabolizing enzymes in the endocannabinoid system.[21] Moreover a very recent paper[22] shed light on chemo-preventive and curative effects of MAGL inhibition by URB602 in murine models of colorectal cancer *in vivo*.

Structural modifications included isosteric replacement, ring size and para substitution of the biphenyl moiety with substituents promoting hydrogen bound with MAGL site active, as suggested by molecular modeling[23] (Fig. 1). The biological evaluation includes kinetic enzyme assays and cell-based assays using B16-F10 melanoma cells lysate. Cancer cells are a good model for these studies due to the naturally high expression of MAGL in cancer.[24] Moreover, we replaced carbamate with urea function to investigate what happens by this modification.

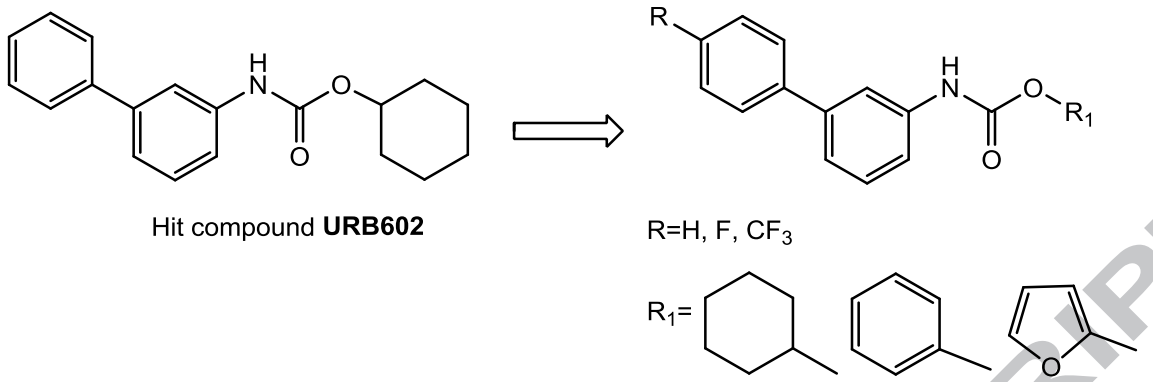

Fig. 1. Structural modifications of hit compound URB602.

2. Results and Discussion

2.1. Chemistry

Starting from the hit compound URB602, we aimed to explore (i) the influence of different para substituent on the biphenyl moiety, (ii) the replacement of cyclohexyl ring by aromatic or heteroaryl moieties, and (iii) the role of carbamate group for the inhibition of MAGL. (Fig. 1). The target compounds **1-2a-c 3a-b** (Scheme 1) were prepared through Suzuki coupling reaction via the key biphenylamine intermediates (**4a-c**), involving phenylboronic acid, 3-bromoaniline and a suitable palladium catalyst. These intermediates were isolated in good yield (58-72%) and were reacted with carbonyldiimidazole (CDI), dimethylaminopyridine (DMAP) and an appropriate alcohol (Scheme 1).

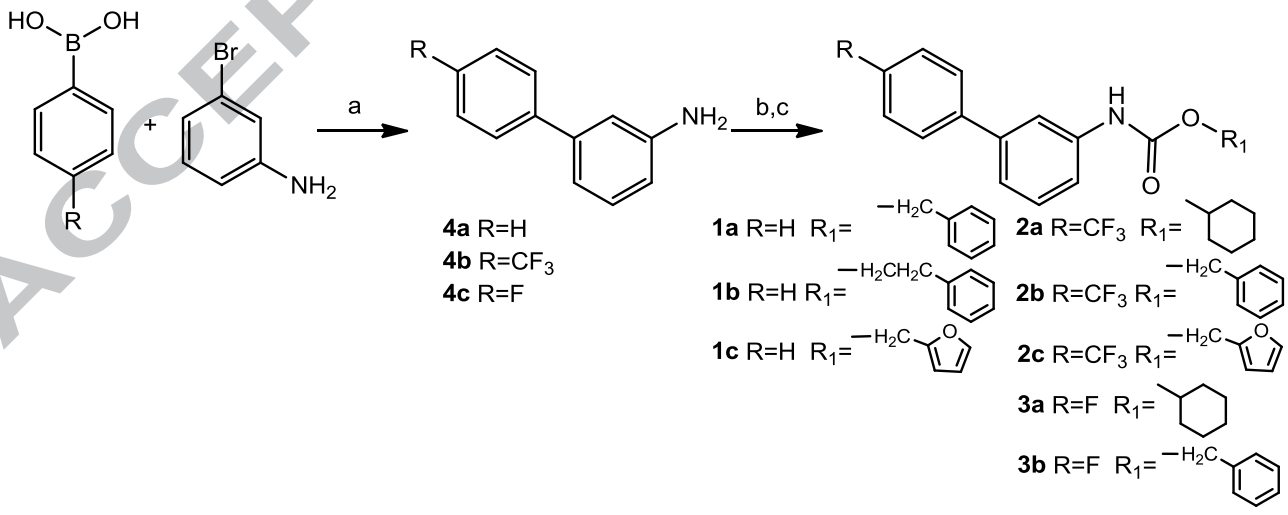

Scheme 1. Synthesis of compounds 1-2a-c 3a-b. Reagents and conditions: (a) $Pd(PPh_3)_4$, Na_2CO_3, CH_3OH, reflux, 12 h; (b) CDI, DMAP, CH_3CN, reflux, overnight; (c) R_1-OH, CH_3CN, reflux.

The urea analogue **5** was synthesized with a one pot reaction of CDI, DMAP and **4a** in dry CH_3CN (Scheme 2). Product **5** precipitates out from the reaction mixture and can be obtained in high purity by filtration (89 % yield).[25]

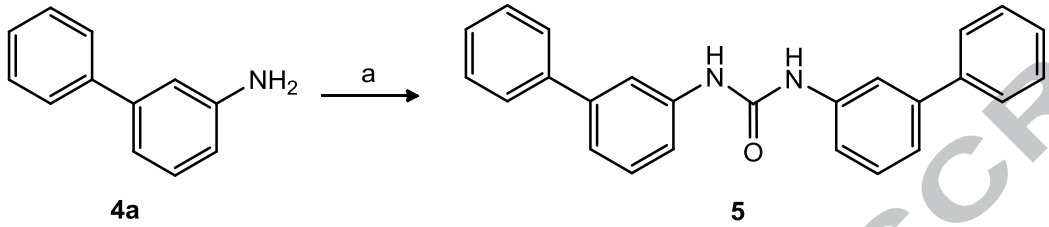

4a **5**

Scheme 2. Synthesis of compound 5. Reagents and conditions: (a) CDI, DMAP, CH_3CN, reflux, overnight.

All the prepared compounds have been characterized by IR, ^{1}H NMR, ^{13}C NMR, as well as elemental analysis. In the ^{13}C NMR spectra of compounds **2a-c**, and **3a-b** carbon-fluorine coupling constants were observed. In ^{13}C NMR spectra of compounds **2a-c** trifluorinated methyl group comes in the aromatic region of the spectrum and fluorinated carbons were often difficult to find due to the 1, 2 and 3 bond *J* coupling to ^{19}F. Indeed the recognition of the multiplicities in the ^{13}C resonances with low signal-to-noise ratios is challenging as the signal is spread over multiple lines and can be buried in the noise.

2.2. Enzyme kinetics studies

The inhibitory activities (IC_{50} values) of the synthesized derivatives were obtained measuring the residual activity of the enzyme with a method based on the enzymatic hydrolysis of a red fluorogenic substrate 7-hydroxyresorufinyl-arachidonate (7-HRA).[26] For our *in vitro* experiments, we chose the commercially available human recombinant enzyme (Cayman Chemical) to have a known reference activity independent from the variability of cell extracts. A series of dilutions of test compounds (1:10) from 1nM to 100 μM (six concentrations in triplicate) was performed using 7-HRA as substrate. The activity data for a handful of compounds at the highest concentration of 100 μM were not determined due to the emergence of solubility issues. 10% DMSO was used in the assay to ensure solubility of the hydrophobic substrate 7-HRA, since hMAGL retains its activity in the presence of DMSO.[27] Furthermore, 7-HRA was stable in 10% DMSO for at least 36 h at room temperature and for at least 6 months at 4 °C.

The unrepeatability of results with the analogue **1c** (Table 1) did not allow to obtain any IC_{50} value for this compound, possibly for severe solubility problems. The results of inhibitory test are summarized in Table 1. In Fig. S1 (Supplementary data) the linear regression between pK_i ($-LogK_i$) and IC_{50} values is plotted from column 2 data. The test results show that compounds **2a-c**, with trifluoromethyl and fluoro substitutions of the aryl group were very active MAGL inhibitors. Whereas, unexpectedly, compound **5** increases activity of MAGL. The EC_{50} value for **5** was reported in Table 1.

Table 1. Chemical structures, calculated partition coefficient (log P), dissociation constant values, and inhibitory activity of compounds **1a-c**, **2a-c**, **3a-b**, **5**.

	LogP[a]	*In silico*	*In vitro*	*Cell based assay*
Compound		Ki[b]	IC_{50}[c] (μM)	IC_{50}[c] (μM)
URB602	5.32	8.9e-06	9.1 ± 0.8[d]	19.79 ± 0.079
1a	4.69	7.4e-06	11.1 ± 2.3	16.48 ± 0.096
1b	5.44	6.0e-06	11.3 ± 1.4	17.14 ± 0.083
1c	4.27	1.3e-05	n.a.	n.a.
2a	6.22	1.6e-05	10.5 ± 2.0	17.40 ± 0.102
2b	5.91	3.0e-06	4.5 ± 0.7	9.414 ± 0.04
2c	5.16	3.3e-06	6.7 ± 0.7	13.19 ± 0.038
3a	5.49	7.7e-06	13.4 ± 0.9	26.69 ± 0.147
3b	5.17	4.8e-06	7.9 ± 0.8	15.61 ± 0.161
		Ki[b]	EC_{50}[e] (μM)	EC_{50}[e] (μM)
5	6.68	2.73e-06	2.8 ± 0.6[e]	5.76 ± 0.02[e]

[a] Calcd. using the Molinspiration Property Engine 2016.10 Program software. [b]The dissociation constant (K_i) values were computed through the binding free energy, according to the following equation: $K_i = e^{\Delta G/RT}$, where *R* represents the gas constant and *T* the absolute temperature, set at 300 K. [c]IC_{50} values are the means of three separate determinations and were determined by more than five concentrations of each inhibitor. [d]The compound URB602 was used as a positive control in the fluorometric assay. [e]EC_{50} values are the means of three separate determinations and were determined by more than five concentrations of compound **5**. Statistical calculation of IC_{50} and EC_{50} values was performed on GraphPad Prism 5.02 (GraphPad Software, Inc.).

2.3. In vitro cell analysis

To assess the inhibitory effect of the molecules on cellular samples, an *in vitro* experiment was performed using cell lysates derived from B16-F10 melanoma, a cancer cell line known to express MAGL.[24,28] B16-F10 melanoma cells lysate was pre-treated for 60 min with DMSO (vehicle) or the compounds at different concentrations in a 96 well plate. Then, the 7-HRA fluorogenic substrate was added to each well and fluorescence was measured every 2.5 min for 2 h. Each molecule was tested in a range of concentration from 0 to 75 μM, as suggested from previous studies on URB602.[29]

The general trend of enzyme inhibition among all molecules is very similar to that of URB602: in terms of potency, they showed activities that are appreciable when administered

at μM concentrations. The molecules **2b** and **2c** showed an increase in activity (IC_{50} = 9.4 μM ± 0.04 and 13.2 μM ± 0.038 respectively) that is significantly different from URB602 (IC_{50} = 19.8 μM ± 0.079) (Supplementary Table 1 and Fig. S2). Ureic molecule **5** showed no activity at all as inhibitor but seemed to increase the activity of the enzymatic apparatus (Supplementary Fig. S2).

The reported calculated partition coefficient between water and octanol (log P) for the compound **1a-c, 2a-c, 3a-b, 5**. (Table 1) shows that these molecules have comparable lipophilicity, so the ability to enter lipid membranes by passive diffusion are good for all compounds. For the two compounds, i.e. **2b** and **2c**, with the best IC_{50} *in vitro* and in cell based assay, the ability to inhibit MAGL was tested also in intact cells. Both the compounds were able to significantly reduce MAGL activity at the concentration of 10 μM (Supplementary Fig. S2b).

Given the potential of inhibiting MAGL as antitumor therapeutic strategy, we tested *in vitro* the cytotoxic capacity of the synthesised compounds. To this end B16-F10 cells were treated with 10 μM of each compound for 48 h and cell proliferation was analysed by flow cytometry using the fluorescent dye Cyto Track red.[30] As shown in Fig. 2a at 10 μM only the compounds **2b** and **2c** were able to inhibit cell proliferation significantly, with **2c** showing the highest activity against B16-F10; all the other compounds (**1a**, **1b**, **2a**, **3a** and **3b**), including URB602 did not modified the proliferation index of B16-F10 cells with respect to the vehicle (DMSO) treated cells. These results demonstrate the effective anti-proliferative role of compounds **2b** and **2c** in melanoma cells. For these two compounds, we then analysed the ability to induce cell death, comparing them with URB602. Flow cytometry analysis of phosphatidylserine exposure on the outer leaflet of the plasma membrane (a typical feature of apoptotic cell death) revealed that 10 μM of **2b** and **2c** for 48 h induced a significant increase in the Annexin V+ cells (Fig. 2b) no apoptosis was induced by the administration of URB602. Of notice, exposure to 10 μM of **2c** for 48h resulted in a massive induction of cell death both by apoptosis (c.a. 65% of cells) and necrosis (c.a. 15% of cells). The hydrolysis of 2-AG is catalysed not only by MAGL, but also by two novel serine hydrolases, alpha-beta-hydrolase domain 6 and 12 (ABHD6 and ABHD12).[5] In B16-F10 the expression of MAGL and ABHD6, evaluated by real-time PCR was very similar (ΔCT=11.05±0.92 for MAGL and ΔCT=10.73±0.52 for ABHD6), while ABHD12 was almost undetectable (ΔCT=16.84±2.28). To date, little is known about the role of ABHD6 in tumors. This serine hydrolase has been found differentially expressed among various tumor cell lines,[31] but its down-regulation seems not to be related with inhibition of tumor growth.[32] Taken together these data,

complemented by the knowledge that MAGL accounts for approximately 85% of hydrolysis of 2-AG and ABHD6 and ABHD12 are responsible only for almost the remaining 15% of hydrolysis,[5] suggested that the effect of compounds **2b** and **2c** is dependent on MAGL inhibition. This was supported by the effect of decreasing doses of the compound **2c** (75 nM and 35 nM). Indeed, the compounds were synthetized based on a specific MAGL inhibitor and reducing the dose should guarantee the interaction with the highly affine receptor. The two low doses of **2c** were still able to inhibit cell proliferation and trigger cell death via apoptosis in a dose-dependent manner (Fig. 2c and 2d).

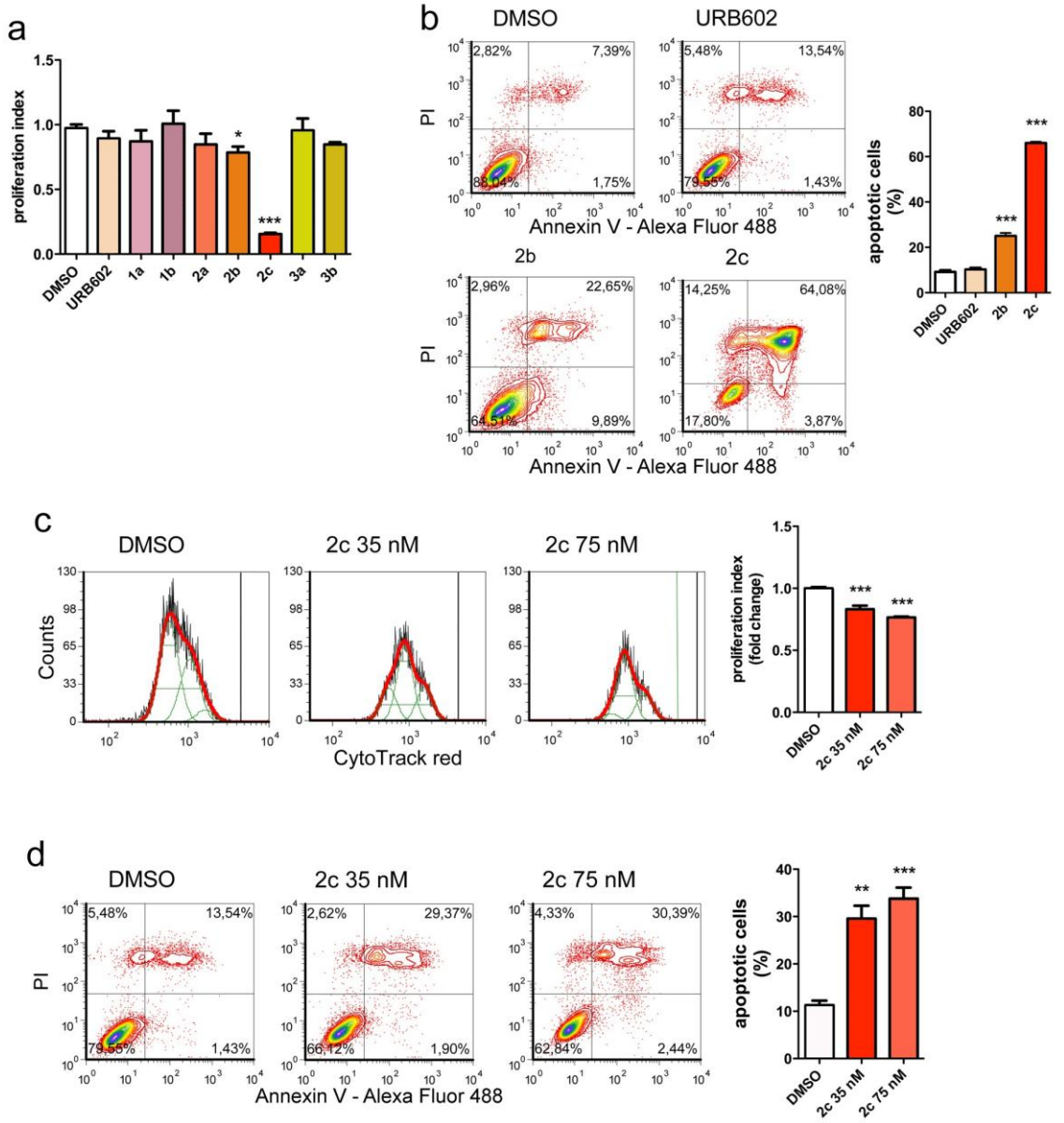

Fig. 2. Effect of synthetic compounds on cell proliferation and apoptosis. (a) B16-F10 cells were cultured in the presence of 10 µM of each compound for 48 h. Cell proliferation was analysed by flow cytometry. Data are expressed as the fold change of proliferation index over control (DMSO) (n = 3). *$p < 0.05$ and ***$p < 0.0001$ vs the respective control. (b) B16-F10 cells were treated with 10 µM of compounds **2b** and **2c** for 48 h. Cell death was analysed by

flow cytometry. Images on the left are representative contour plots of Annexin V-FITC/PI staining. The graph on the right show the mean ± S.E.M. percentage of apoptotic cells (Annexin V^+/PI^- + Annexin V^+/PI^+ fraction; the Annexin V^-/PI^+ fraction, regarded as necrotic stage, was excluded) for 3 independent experiments. ***$p < 0.0001$ vs the respective control. (c, d) Evaluation of cell proliferation (c) and apoptosis (d) after treatment of cells with 35 nM and 75 nM of the compound **2c** for 48 h. Images on the left are representative proliferation (c) and contour plots (d). The vertical black line in the proliferation plots represents the undivided cell peak used as point of reference. Data in the graphs on the right are expressed as the fold change of proliferation index over control (DMSO treated cells) (c) and % of apoptotic cells (d) ($n = 3$). **$p < 0.001$ and ***$p < 0.0001$ vs the respective control.

To further investigate the dependence of the cytotoxic effect of compound **2c** by MAGL inhibition we evaluated two cell lines expressing different levels of the three enzymes (Fig. 3a), the human breast adenocarcinoma MCF7 and embryonic kidney HEK293T. As shown in Fig. 3a, MCF7 expressed MAGL at higher levels with respect to HEK293T, while ABHD6 and ABHD12 were expressed at significantly lower levels. As result, MCF7 were more sensible to apoptosis induced by compounds **2c** with respect to HEK293T (Fig. 3b), thus indicating a predominant role for MAGL inhibition in the induction of apoptosis. The cytotoxic effect on MCF7 was further confirmed by the evaluation of MAGL activity. In the presence of both compounds **2b** and **2c** enzyme activity was indeed inhibited in a significant manner (Fig. 3c). The lower sensitivity of MCF7 to compound **2c** with respect to B16-F10 may be due to different mechanisms of chemoresistance, as for instance the lack of expression of caspase 3 in this cell line.[33] To investigate whether the inhibition of MAGL activity by **2c** accounted for its protective effect, we treated MCF7 cells with the compound alone and together with JZL184, a known specific inhibitor of MAGL (Supplementary Fig. S3a). The two molecules induced apoptosis at the same levels when administered alone or in combination, thus corroborating the idea that they act through the same target i.e. MAGL (Supplementary Fig. S1a). These data were also confirmed by the fact that both oleoyl ethyl amide (OEtA), an inhibitor of fatty acid amide hydrolase enzyme (FAAH) and KT195, an inhibitor of ABHD6, were not able to induce MCF7 apoptosis (Supplementary Fig. S3b).

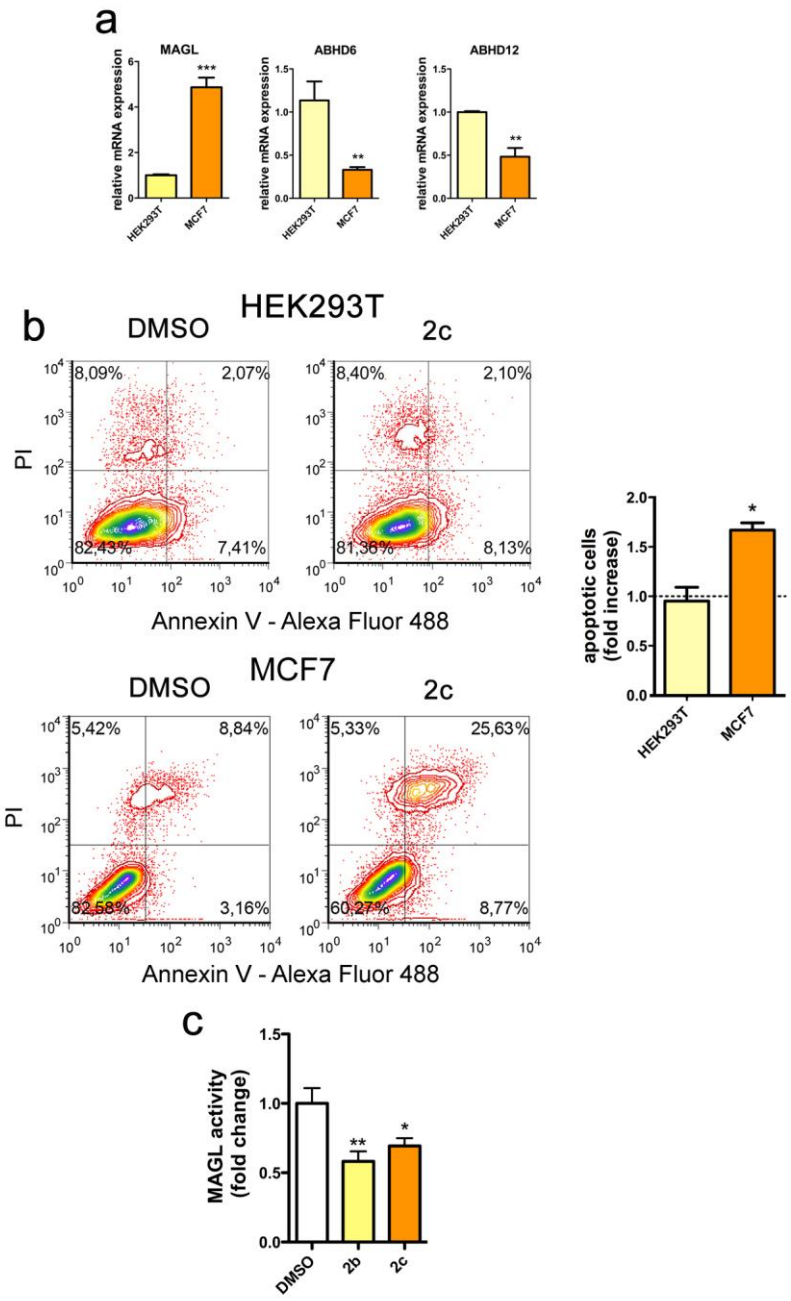

Fig. 3. (a) evaluation of MAGL, ABHD6 and ABHD12 expression in MCF7 and HEK293T human cell lines. Data are expressed as fold change vs HEK293T (n=4). $^{**}p < 0.001$; $^{***}p < 0.0001$ vs HEK293T. (b) Cell death analysis by flow cytometry. Right panel: representative contour plots of Annexin V-FITC/PI staining of HEK293T and MCF7 cells treated with 10 µM of compound **2c** for 48 h (n=3). The data in the graph are expressed as means ± S.E.M.. $^{*}p < 0.05$ vs DMSO treated cells. (c) MCF7 cells were cultured for 6 h in the presence of the compounds 2b and 2c (10 µM). MAGL activity was measured on total cell lysate. $^{*}p < 0.05$; $^{**}p < 0.001$ vs DMSO treated cells.

All these data combined with the results obtained in the *in vitro* experiments (Table 1) and with the knowledge that URB602 selectively block MAGL[29] seem to indicate that compounds **2b** and **2c** induce cell death through the inhibition of MAGL.

2.4. Study of inhibitor selectivity

To assess the selectivity of more active compounds (**2b, 2c**) as MAGL inhibitors, we evaluated also their activity toward fatty acid amide hydrolase enzyme (FAAH), the other major endocannabinoids hydrolytic enzyme. First the fluorogenic probe for FAAH, arachidonoyl-aminomethylcoumarine amide (AAMCA), was synthesized starting from arachidonic acid and 7-amino-4-methyl coumarine, by a coupling reaction.[34] NMR confirmed the structure and purity grade of the product (Supplementary data).

Inhibitor activity of **2b** and **2c** has been assessed by a well-known fluorescence based method on hFAAH[35] and oleoyl ethyl amide[36] has been selected as positive control. In our experimental conditions compounds **2b** and **2c**, at cells bioactive concentration of 10 μM, showed an inhibitory activity of 15% and 10% respectively while OEtA displayed 99% inhibition of hFAAH hydrolytic activity (Supplementary fig.S4).

2.5. Molecular mechanism of MAGL inhibition

Fig. 4 shows the MAGL binding site, according to the MOE Site Finder, a region located in the near proximity of the catalytic active site that has already been described by Szabo and colleagues[21] as the most likely binding site for the interaction with potential inhibitors.

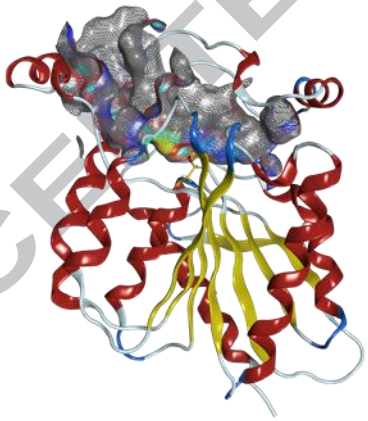

Fig. 4. MAGL binding site according to the MOE Site Finder. 3JW8 is represented as ribbon and the binding site as a gray shaded molecular surface.

Table 1 reports the dissociation constant value (K_i) for the top-scoring pose of each tested inhibitor, showing the ability of all the tested compounds to bind and block the MAGL active site. Globally, our docking simulations provided overlapping poses for all the tested compounds and a good superposition of their common functional groups, confirming the accuracy of this approach.

At an atomistic level, the top-scoring pose of the parent compound URB602 well fits the enzyme binding site, as also suggested by its good Ki value, in agreement with the experimental IC_{50} (Fig. 5a,b). The carbamate group lies close to the catalytic Ser132, confirming that the actual mechanism of these compounds is the inhibition of MAGL activity. Due to its nonpolar nature, URB602 establishes interactions with the hydrophobic residues that characterize the MAGL pocket. In detail, the mono-substituted aromatic ring of URB602 engages Leu215 and Ile189 sidechains via C-H-π interactions. Moreover, the carbonyl oxygen of the ligand interacts with Ala61 backbone via H-bond.

Compound **2b**, associated to the best K_i value, also showed the best inhibitory activity using the fluorescent method previously described.

Fig. 5a,c reports the MAGL::**2b** interactions: the molecule accommodates in proximity of hydrophobic residues such as Leu and Ile; in particular, as for URB602, an arene-H interaction occurs between the side chain of Ile189 and the biphenyl group, so that the trifluoromethyl substituent is stretched toward Ile189 and Leu21. The benzyl ring occupies the same region of the URB602 cyclohexyl ring, and the two carbamate groups are superposed. Moreover, the ligand carbonyl oxygen is placed in proximity of Met133 and Ala61, establishing two H-bond interactions with their backbones.

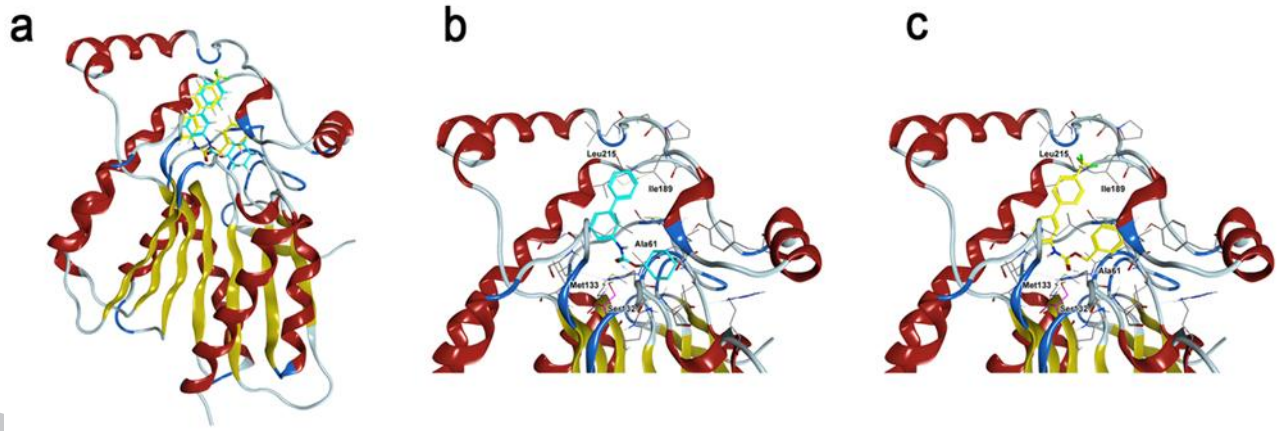

Fig. 5. Molecular recognition mechanism of MAGL inhibitors. (a) URB602 and compound **2b** docked to MAGL are represented in cyan and yellow stick, respectively. MAGL is represented as ribbon. (b) Detailed molecular interactions between MAGL residues and URB602 (b) and compound **2b** (c) in the catalytic pocket. Catalytic Ser132 is highlighted in magenta.

Overall, our *in silico* results suggest that the introduction of classical small lipophilic substituent on the biphenyl group, like fluorine or trifluoromethyl, improves the affinity for the enzyme, likely due to the hydrophobic environment of the pocket. Similarly, the replacement of the aliphatic cyclohexyl group with an aromatic one produces a more efficient

interaction between the potential inhibitor and the enzyme, especially when the carbamate and the ring are separated by a single carbon atom chain, while elongating the alkyl chain does not result in an improved affinity.

Common features of the tested inhibitors in the binding MAGL pocket are recapitulated by the proposed pharmacophoric model. In detail, an acceptor, a donor, an aromatic and a hydrophilic feature are highlighted in Fig. 6 as spheres. This model has been built keeping into account not only the common feature of the functional groups but also the activity for each inhibitor. No differences exist between two different models based on activities on purified MAGL and cultured cells. All the pharmacophoric features are present in the 100% of the inhibitors compounds, with an alignment score of 7.5, and seem to be crucial for the activity of this series of compounds. By definition, only the inactive compound does not match the pharmacophoric query.

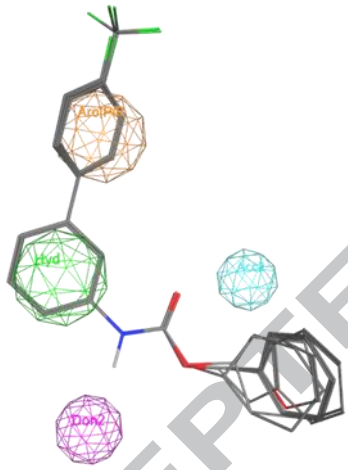

Fig. 6. Pharmacophoric model and structure activity relationship for MAGL inhibitors. The pharmacophore features are represented as colored spheres: orange for aromatic or Pi ring center, green for hydrophobic, cyan for H-bond acceptor and magenta for H-bond donor.

2.6. Molecular mechanism of MAGL activation

During this synthetic project a symmetric compound **5** (Scheme 2) was designed, synthesized and tested, and it was demonstrated to be an interesting MAGL activator. In order to better understand its activating mechanism at a molecular level, we checked the 3D MAGL structure (RCSB PDB: 3JV8[23]) and we looked for all the other crystallographic structures of MAGLs, identifying a human form co-crystallized with an irreversible inhibitor (RCSB PDB: 3JWE[23]). A careful inspection of both the structures revealed a molar ratio of 4 molecules of 2-methyl-pentane-2,4-diol (MPD) per 1 enzyme in 3JV8 and a molar ratio of 2 molecules of SAR per 1 enzyme in 3JVE.[23] In detail, in 3JV8 crystal, approx. two MPD molecules occupy the

catalytic site, while two other molecules are located in a second pocket (external binding site), close to the α-helix 4 of the lid domain,[23] suggesting that the MAGL secondary pocket is not a crystallographic artifact. In 3JVE, one SAR molecule covalently binds Ser132 of the catalytic triad, after the elimination of triazole as a leaving group, while the second one is non-covalently bound in the second pocket in contact with the α-helix 4. Fig. 7a shows the superposition between 3JV8 and 3JVE binding sites in which MPD and SAR molecules occupy both active and secondary pockets with very similar distribution in space.
These observations suggested us that our activator could preferentially bind to this second pocket, modifying the orientation of the α-helix 4, and consequently increasing the accessibility of substrates to, and their affinity for the catalytic site.
A first run of molecular docking was carried out on this crystallographic structure, after removing both the two inhibitor molecules. Our activator was docked on the 3JWE 3D structure, setting the whole protein as binding site. We obtained two different clusters of accepted solutions. The most energetically favored pose belongs to the cluster located in the external binding site, and has a binding free energy of -6.94 kcal/mol with an associated affinity value of -7.56 kcal/mol; whereas the top-scoring pose belonging to the cluster located into the catalytic site is characterized by less favorable energetic values: -6.88 kcal/mol and -6.97 kcal/mol, respectively (Fig. 7b).

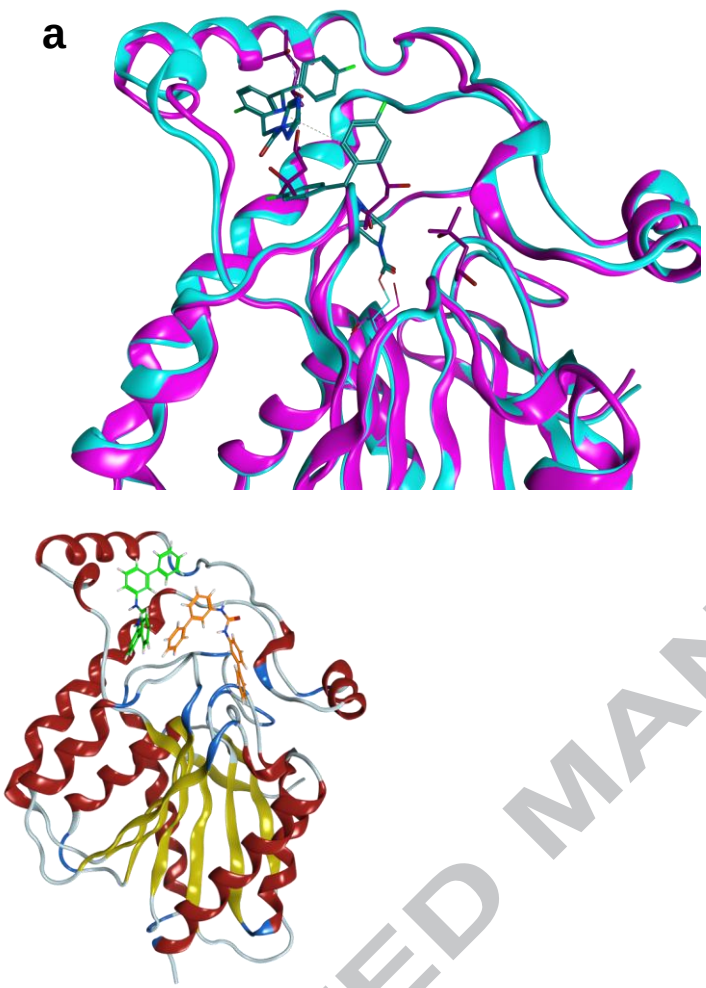

Fig. 7. MAGL binding site. (a) Focus on two different crystals of MAGL binding site: in magenta, crystal structure of 3JW8, with 4 co-crystallized MPD molecules; in light blue, crystal structure of 3JWE, with 2 co-crystallized SAR molecules. (b) Superposition of two activator::MAGL (3JWE) complexes: in orange, the activator in placed in the enzyme catalytic site; in green, the activator in the external binding site.

Furthermore, a reference substrate, 2-AG, was docked both on an apo- and on a holo-MAGL form bound to the studied activator. The latter form was generated by molecular docking of the activator on the MAGL external binding site. The solutions were characterized by the following affinity values: -8.49 kcal/mol, and -9.09 kcal/mol, for the apo- and holo-MAGL form (Fig. 8), respectively. This result suggests a higher affinity for this reference substrate when our activator is bound to the MAGL external binding site.

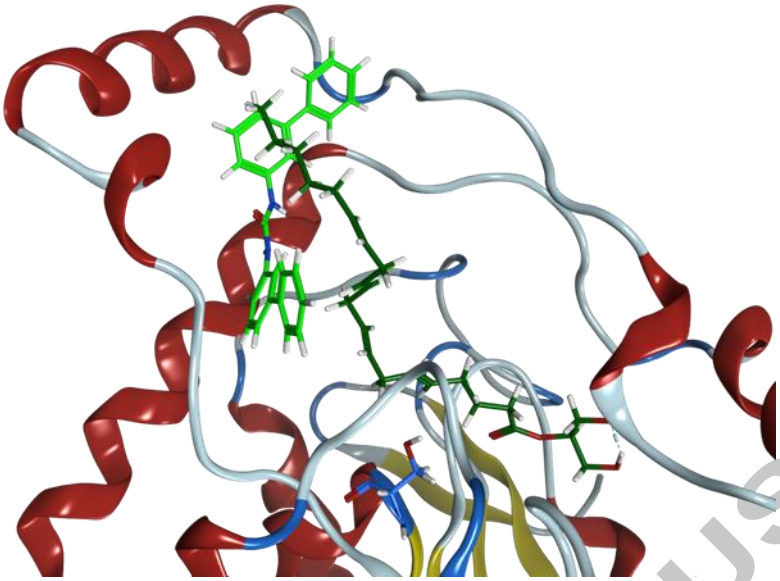

Fig. 8. MAGL can contemporarily bind out activator and a model substrate. Top scoring docking pose of 2-AG (dark green) with respect to the activator::MAGL complex (PDB: 3JWE) in the catalytic site. Ser132 of the catalytic triad is depicted in blue.

3. Conclusions

In this study, we have designed and synthesized a new series of carbamates as MAGL inhibitors. The best activity values were obtained with compounds **2b**, **2c**, and **3b** (IC_{50} 4.5, 6.7, and 7.9 μM, respectively) bearing the 4'-trifluoromethyl substitution of the biphenyl moiety and aromatic functionality at the oxygen side of the carbamate molecule. Compounds containing fluoro moieties on the 4' position of biphenyl ring resulted in a decreased potency for hMAGL enzyme. Molecular modelling studies further demonstrated that compound **2b** establishes favorable interactions, due to its improved lipophilicity, within the active site of hMAGL, rich of hydrophobic residues that participate in the molecular recognition mechanism.

Taken together, docking scores confirm that an increase of the hydrophobic and aromatic functional groups of the inhibitors improves their affinity for the enzyme. Our molecular modelling strategy allowed us to develop a first pharmacophoric model, connecting the structure and activity relationships of the investigated series of inhibitors. The characterization of further MAGL active compounds is mandatory for refining our structure and activity relationship model in order to identify novel hit compounds.

In vitro experiments on cancer cells demonstrated that compounds **2b** and **2c**, were able to block cell proliferation as well as to induce cell death via apoptosis thus indicating this molecule as very promising anti-cancer drug. Moreover in present studies, three series of data, determined separately, with hMAGL, with cell lysate and modeling studies are in agreement

and gave precise indications that compound **5** is an activator, allowed us to identify, to our knowledge, first MAGL activator posing the bases for the development of novel enzymatic MAGL modulators with promising applications. Further studies are needed to better understand this activity.

4. Experimental section

4.1. Chemistry

All of the reagents and solvents, analytically pure, were obtained from commercial sources and used without further purification. Reaction progress was monitored by TLC on pre-coated silica gel plates (Kieselgel 60 F254, Merck) and visualized by UV254 light. Flash column chromatography was performed on silica gel (particle size 40-63 μm, 60 Å). Anhydrous solvents were obtained by passing solvents through activated alumina columns. When stated, reactions were carried out under an inert atmosphere. Purity of all products (≥ 98 %) was verified by thin-layer chromatography and NMR measurements. Elemental analyses were obtained for all intermediates and are within ± 0.4% of theoretical values. Human recombinant C-terminal hexahistidine-tagged protein expressed in *E. coli* MAGL (hMAGL), human recombinant C-terminal His-tagged protein expressed in Sf21 cells (hFAAH) and oleoylethylamide (OEtA) were purchased from Cayman Chemical.

Melting points were determined with a Stuart Scientific SMP3 melting point apparatus. ^{1}H NMR spectra were recorded in $CDCl_3$ (isotopic enrichment 99.95%) or DMSO-*d6* (isotopic enrichment 99.98%) or CD_3OD (isotopic enrichment 99.98%), solutions at 300 K using a Bruker AVANCE 500 instrument (500.13 MHz for 1H, 125.76 MHz for 13C) using 5 mm inverse detection broadband probes and deuterium lock. Chemical shifts (δ) are given in parts per million (ppm) and were referenced using residual signals of the solvent as internal standard (^{1}H: $CHCl_3$, 7.26 ppm; CD_3OD, 3.30 ppm; DMSO, 2.49 ppm. ^{13}C: $CDCl_3$, 77.0 ppm; CD_3OD, 47.6 ppm, central line; DMSO-*d6*, 39.5 ppm). Coupling constants (J) are in hertz (Hz) and the experimental error in the measured ^{1}H-^{1}H coupling constants is ± 0.5 Hz. The results are presented as the chemical shift in ppm, number of protons, multiplicity, J values in Hertz, proton position, or carbon position. The splitting pattern abbreviations are as follows: s, singlet; d, doublet; t, triplet; q, quartet; m, multiplet, and bs, broad signal. For two-dimensional experiments, Bruker microprograms using gradient selection (gs) were applied. IR spectra were determined on a Jasco FTIR 4100 spectrometer as a thin film on NaCl plates and were expressed in cm^{-1} scale.

*4.1.1. General procedure for the Suzuki coupling reaction to obtain compounds **4a-c**.* To a solution of phenylboronic acid (4.0 mmol) in 10 mL of MeOH, Na_2CO_3 (8.0 mmol) and 3-bromoaniline (4.0 mmol) were added sequentially. To this suspension, Pd tetrakis (0.14 mmol) was added and the reaction was heated to reflux for 12 h; the suspension was cooled at room temperature, diluted with MeOH and the black precipitate was removed by filtration. The filtrate was diluted with water and extracted with CH_2Cl_2 (3 x 10 ml). The organic phase was dried on Na_2SO_4 and concentrated under reduced pressure.

*4.1.2. [1,1'-biphenyl]-3-amine (**4a**).* The product, prepared starting from phenylboronic acid and 3-bromoaniline and purified by chromatography on silica gel (petroleum ether:CH_3OH, 80:20 v/v) was obtained as a white solid in 72% yield. mp: 29-30.5 °C (lit.[37] 28-30 °C); ^{1}H NMR ($CDCl_3$) δ: 7.58 (2H, d, J=7.4 Hz, 2', 6'-H), 7.43 (2H, dd, J=7.4, 7.4 Hz, 3', 5'-H), 7.35 (1H, t, J=7.4 Hz, 4'-H), 7.24 (1H, dd, J=7.6, 7.6 Hz, 5-H), 7.01 (1H, ddd, J=7.6, 1.0, <1.0 Hz, 6-H), 6.92 (1H, dd, J=1.3, <1.0 Hz, 2-H), 6.69 (1H, ddd, J= 7.8, 1.3, 1.0 Hz, 4-H), 3.75 (2H, s, 7-NH_2). ^{13}C NMR δ: 146.7 (3), 142.5 (1), 141.4 (1'), 129.7 (5), 128.6 (3', 5'), 127.2 (6', 2'), 127.1 (4'), 117.7 (6), 114.1 (4), 114.0 (2).

*4.1.3. 4'-(trifluoromethyl)-[1,1'-biphenyl]-3-amine (**4b**).* The product, prepared starting from 4-(trifluoromethyl)phenylboronic acid and 3-bromoaniline, purified by chromatography on silica gel (petroleum ether:CH_3OH, 70:30 v/v), was obtained as a white solid in 58% yield. mp: 90-91 °C (lit.[38] 91-92 °C); ^{1}H NMR ($CDCl_3$) δ:7.41-7.68 (4H, m, 2″, 3″, 5″and 6″), 5.29 (1H, dd, J=7.9 Hz, 5-H), 5.60 (1H, dd, J=1.3, <1.0 Hz, 2-H), 5.59 (1H, ddd, J=7.5, 1.3, 1.3 Hz, 6-H), 5.37 (1H, ddd, J= 7.5, 1.3, <1.0 Hz, 4-H); ^{13}C NMR δ: 146.9 (3), 144.9 (1'), 140.9 (1), 129.9 (5), 129.2 (q, $^2J_{C-F}$ = 32.6 Hz, 4'), 127.3 (2', 6'), 126.2 (q, $^1J_{C-F}$ = 271.6 *C*F_3), 125.6 (q, $^3J_{C-F}$ = 4.1 Hz, 3', 5'), 117.7 (6), 114.6 (4), 113.8 (2).

*4.1.4. 4'-fluoro-[1,1'-biphenyl]-3-amine (**4c**).* The product, prepared starting from 4'-fluorophenylboronic acid and 3-bromoaniline and purified by chromatography on silica gel (petroleum ether: CH_3OH, 70:30 v/v), was obtained as a white solid in 68% yield. mp: 29-30.5 °C (lit.[39] 28-30 °C); ^{1}H NMR (CD_3OD) δ: 7.59-7.55 (2H, AA′ part of AA′BB′ system, 2'- and 6'-H), 7.17 (1H, dd, J=7.8, 7.8 Hz, 5-H), 7.16-7.11 (2H, BB′ part of AA′BB′ system,, 3'- and 5'-H), 6.96 (1H, dd, J=1.3, 1,3 Hz, 2-H), 6.91 (1H, ddd, J=7.8, 1.3, 1.3 Hz, 6-H), 6.72

(1H, ddd, J=7.8, 1.3, 1.3 Hz, 4-H); ^{13}C NMR δ: 162.3 (d, $^{1}J_{C-F}$ = 244.5 Hz, 4'), 147.8 (3), 140.9 (1), 137.9 (d, $^{4}J_{C-F}$ = 2.9 Hz, 1'), 129.1 (5), 128.2 (d, $^{3}J_{C-F}$ = 8.0 Hz, 2', 6'), 116.5 (6), 114.8 (d, $^{2}J_{C-F}$ = 21.5 Hz, 3', 5'), 114.2 (4), 113.6 (2).

4.1.5. General procedure for the preparation of compounds ***1-2a-c, 3a-b.*** A stirred solution of the previously obtained amine (1 mmol), CDI (4 mmol, 0.648 g), and DMAP (0.2 mmol, 0.024 g) in CH_3CN (8 mL) was heated at 100 °C for 15 h under N_2 atmosphere. Then a solution of the suitable alcohol (1.2 mmol) in CH_3CN (1 mL) was added. The mixture was stirred at 100 °C for 8 h and concentrated.

*4.1.6. Benzyl [1,1'-biphenyl]-3-ylcarbamate (**1a**).* The product, prepared starting from **4a** and phenyl methanol and purified by chromatography on silica gel (petroleum ether:EtOAc, 90:10 v/v), was obtained as a white solid in 62% yield. mp: 73.2-73.9 °C. TLC (petroleum ether: EtOAc, 95:5 v/v): Rf=0.33; IR (Nujol): 3324, 1941, 1700, 1550, 1376, 1274, 1076, 754, 696 cm^{-1}; ^{1}H NMR ($CDCl_3$) δ: 7.68 (1H, bs, 2-H), 7.61 (2H, bd, J=7.3 Hz, 2', 6'-H), 7.47-7.37 (10H, m, 3', 4', 5', 5, 6, 5 x Ar-H), 7.33 (1H, dd, J=8.7, 1.8 Hz, 4-H), 6.79 (1H, bs, NH), 5.26 (2H, s, -CH_2); ^{13}C NMR δ: 153.4 (*C*O), 142.3 (1), 140.7 (1'), 138.2 (3), 136.1 (1''), 129.5, 128.8, 128.7, 128.4, 128.4, 127.5, 127.2 and 122.4 (*C*-Ar), 67.1 (*C*H_2). Anal. Calcd. for $C_{20}H_{17}NO_2$: C, 79.19; H, 5.65; N, 4.62. Found: C, 79.30; H, 5.47; N, 4.60.

*4.1.7. Phenethyl [1,1'-biphenyl]-3-ylcarbamate (**1b**).* The product, prepared starting from **4a** and phenylethanol and purified by chromatography on silica gel (petroleum ether:EtOAc, 80:20 v/v), was obtained as a white solid in 74% yield. mp 98.2-99.4 °C. TLC (petroleum ether: EtOAc, 80:20 v/v): Rf=0.41; IR (Nujol): 3414, 1955, 1729, 1573, 1376, 1275, 1078, 754, 699 cm^{-1}; ^{1}H NMR ($CDCl_3$) δ: 7.66 (1H, bs, 2-H), 7.61 (2H, d, J=7.6 Hz, 2', 6'-H), 7.46 (2H, t, J=7.6 Hz, 3', 5'-H), 7.42-7.27 (10H, m, 3', 4', 5', 5, 6, 5 x Ar-H), 6.69 (1H, bs, NH), 4.45 (2H, t, J=7.0 Hz, -CH_2), 3.04 (2H, t, J=7.0 Hz, -CH_2). ^{13}C NMR δ: 153.5 (*C*O), 142.3 (1), 140.7 (1'), 138.3 (1''), 137.8 (3), 129.5, 128.9, 128.8, 128.6, 127.5, 127.2, 126.7 (*C*-Ar), 65.7 (*C*H_2), 35.5 (*C*H_2). Anal. Calcd. for $C_{21}H_{19}NO_2$: C, 79.47; H, 6.03; N, 4.41. Found: C, 79.57; H, 6.12; N, 4.36.

*4.1.8. Furan-2-ylmethyl [1,1'-biphenyl]-3-ylcarbamate (**1c**).* The product, prepared from **4a** and 2-furfuryl alcohol and purified by chromatography on silica gel (petroleum ether:EtOAc,

90:10 v/v) was obtained as an oil 68% yield. TLC (petroleum ether: EtOAc, 75:25 v/v): Rf=0.61; IR (Nujol): 3330, 1934, 1737, 1598, 1265, 1156, 744, 704 cm^{-1}; ^{1}H NMR ($CDCl_3$) δ: 7.67 (1H, bs, 2-H), 7.60 (2H, d, J=7.8, 2′, 6′-H), 7.48 (1H, dd, J=1.9, <1 Hz, 5′′-H), 7.46 (2H, dd, J=7.8, 7.8 Hz, 3′, 5′-H), 7.41-7.36 (3H, m, 4-, 5-, 4′-H), 7.33 (1H, ddd, J=7.1, 1.7, 1.7 Hz, 6-H), 6.78 (1H, ds, NH), 6.50 (1H, dd, J=3.3, <1.0 Hz, 3′′-H), 6.41 (1H, dd, J=3.3, 1.9 Hz, 4′′-H), 5.21 (2H, s, CH_2).^{13}C NMR δ: 153.0 (*C*O), 149.6 (2′′), 143.4 (5′′), 142.3 (1), 140.7 (1′), 138.1 (3), 129.4, 128.8, 127.5, 127.2, (5, 2′, 3′, 4′, 5′, 6′), 122.5 (6), 117.6 (2, 4), 110.8 (4′′), 110.6 (3′′), 58.8 (*C*H_2). Anal. Calcd. for $C_{18}H_{15}NO_3$: C, 73.71; H, 5.15; N, 4.78. Found: C, 73.86; H, 5.26; N, 4.60.

*4.1.9. Cyclohexyl (4'-(trifluoromethyl)-[1,1'-biphenyl]-3-yl)carbamate (**2a**)*. The product, prepared starting from **4b** and cyclohexanol and purified by chromatography on silica gel (petroleum ether:EtOAc, 90:10 v/v), was obtained as a white solid in 74% yield. mp 124.8-126.2 °C. TLC (Rf=0.62, petroleum ether: EtOAc, 80:20 v/v). IR (Nujol): 3342, 1912, 1697, 1548, 1329, 1235, 1118, 1070, 781 cm^{-1}; ^{1}H NMR ($CDCl_3$) δ: 7.78 (1H, bs, 2-H), 7.73-7.69 (4H, m, 2', 3', 5' and 6'-H), 7.42 (1H, dd, J=7.8, 7.8 Hz, 5-H), 7.36 (1H, ddd, J=7.8, 1.4, 1.4 Hz, 4-H), 7.31 (1H, ddd, J=7.8, 1.4, 1.4 Hz, 6-H), 6.69 (1H, s, NH), 4.83-4.77 (1H, m, 1′′-H), 2.00-1.98 (2H, m, 2′′-H_{eq} and 6′′-H_{eq}), 1.80-1.76 (2H, m, 3′′-H_{eq} and 5′′-H_{eq}), 1.62-1.59 (1H, m, 4′′-H_{eq}), 1.54-1.39 (4H, m, 2′′-H_{ax} , 3′′-H_{ax}, 5′′-H_{ax} and 6′′-H_{ax}), 1.34-1.26 (1H, m, 4′′-H_{ax}); ^{13}C NMR δ: 153.2 (*C*O), 144.3 (1'), 140.7 (1), 138.8 (3), 129.6 (5), 129.4 (q, $^{2}J_{C-F}$ = 32.2 Hz, 4'), 127.4 (2′, 6′), 126.4 (q, $^{1}J_{C-F}$ = 270.2 *C*F_3), 125.7 (q, $^{3}J_{C-F}$ = 4.2 Hz, 3', 5'), 122.1 (6), 118.2 (4), 117.4 (2), 73.9 (1′′), 31.9 (2′′, 6′′), 25.4 (4′′), 23.8 (3′′, 5′′). Anal. Calcd. for $C_{21}H_{22}F_3NO_2$: C, 66.83; H, 5.88; N, 3.71. Found: C, 66.96; H, 5.90; N, 3.84.

*4.1.10. Benzyl (4'-(trifluoromethyl)-[1,1'-biphenyl]-3-yl)carbamate (**2b**)*. The product, prepared starting from **4b** and phenyl methanol and purified by chromatography on silica gel (petroleum ether:EtOAc, 80:20 v/v), was obtained as a white solid in 84% yield. mp 114.6-116.0 °C. TLC (petroleum ether: EtOAc, 80:20 v/v): Rf=0.59; IR (Nujol): 3292, 1935, 1687, 1574, 1542, 1330, 1273, 1114, 1072, 782 cm^{-1}; ^{1}H NMR ($CDCl_3$) δ: 7.75 (1H, bs, 2-H), 7.70 (4H, m, 2', 3', 5' and 6'-H), 7.46-7.37 (8H, m, 4, 5, 6, 2′′, 3′′, 4′′, 5′′and 6′′), 7.32 (1H, ddd, J=7.9, 1.2, 1.2 Hz, 6-H), 6.80 (1H, s, NH), 5.27 (2H, s, C*H*$_2$); ^{13}C NMR δ: 153.3 (*C*O), 144.3 (1'), 140.8 (1), 138.5 (3), 135.9 (1"), 129.7 (5), 129.5 (q, $^{2}J_{C-F}$ = 32.0 Hz, 4'), 128.7, 128.5, 128.4 (2′′, 3′′, 4′′, 5′′, 6′′), 127.5 (2′, 6′), 126.4 (q, $^{1}J_{C-F}$ = 270.2 *C*F_3), 125.7 (q, $^{3}J_{C-F}$ = 4.2 Hz,

3', 5'), 122.5 (6), 118.4 (4), 117.6 (2), 67.2 (*C*H_2). Anal. Calcd. for $C_{21}H_{16}F_3NO_2$: C, 67.92; H, 4.34; N, 3.77. Found: C, 68.02; H, 4.21; N, 3.74.

*4.1.11. Furan-2-ylmethyl 4'-(trifluoromethyl)biphenyl-3-ylcarbamate (**2c**).* The product, prepared starting from **4b** and furfuryl alcohol and purified by chromatography on silica gel (petroleum ether:EtOAc, 80:20 v/v), was obtained as a white solid in 88% yield. mp 119.2-120.0 °C. TLC (petroleum ether: EtOAc, 80:20 v/v): Rf=0.63; IR (Nujol): 3378, 1921, 1696, 1546, 1339, 1275, 1111, 1075, 786 cm^{-1}; ^{1}H NMR ($CDCl_3$) δ: 7.74 (1H, bs, 2-H), 7.72-7.68 (4H, m, 2'- 3'- 5' and 6'-H), 7.48 (1H, dd, J=1.7, <1 Hz, 5"-H), 7.42 (1H, dd, J=7.8, 7.8 Hz, 5-H), 7.36 (1H, bd, J=7.5 Hz, 4-H), 7.33 (1H, ddd, J=7.5, 1.4, 1.4 Hz, 4-H), 6.78 (1H, bs, NH), 6.51 (1H, dd, 3.3, <1 Hz, 4"-H), 6.42 (1H, dd, J=3.3, 1.7 Hz, 3"-H), 5.21 (2H, s, C*H*$_2$); ^{13}C NMR δ: 153.0 (*C*O), 149.4 (2"), 144.2 (1'), 143.4 (5′′), 140.8 (1), 138.3 (3), 129.7 (5), 129.4 (q, $^2J_{C-F}$ = 32.2 Hz, 4′), 127.5 (2′, 6′), 125.7 (q, $^1J_{C-F}$ = 270.6 *C*F_3), 125.3 (q, $^3J_{C-F}$ = 4.0 Hz, 3', 5'), 122.5 (6), 118.4 (4), 117.5 (2), 110.9 (4′′), 110.7 (3′′), 58.8 (*C*H_2). Anal. Calcd. for $C_{19}H_{14}F_3NO_3$: C, 63.16; H, 3.91; N, 3.88. Found: C, 63.32; H, 3.79; N, 3.84.

*4.1.12. Cyclohexyl (4'-fluoro-[1,1'-biphenyl]-3-yl)carbamate (**3a**).* The product, prepared starting from **4c** and cyclohexanol and purified by chromatography on silica gel (petroleum ether:EtOAc, 80:20 v/v), was obtained as a white solid in 84% yield. mp 124.6-125.0 °C. TLC (Rf=0.59, petroleum ether: EtOAc, 80:20 v/v). IR (Nujol): 3338, 1693, 1586, 1548, 1232, 1213, 1174, 1101, 1063, 790 cm^{-1}; ^{1}H NMR ($CDCl_3$) δ: 7.70 (1H, bs, 2-H), 7.59-7.55 (2H, AA′ part of AA′BB′ system, 2'- and 6'-H), 7.38 (1H, dd, J=7.8, 7.8 Hz, 5-H), 7.32 (1H, ddd, J=7.8, 1.4, 1.4 Hz, 4-H), 7.25 (1H, ddd, J=7.8, 1.4, 1.4 Hz, 6-H), 7.15-7.11 (2H, BB′ part of AA′BB′ system, 3'- and 5'-H), 6.68 (1H, s, NH), 4.83-4.75 (1H, m, 1′′-H), 2.01-1.96 (2H, m, 2′′-H_{eq} and 6′′-H_{eq}), 1.81-1.76 (2H, m, 3′′-H_{eq} and 5′′-H_{eq}), 1.62-1.57 (1H, m, 4′′-H_{eq}), 1.54-1.38 (4H,m, 2′′-H_{ax}, 3′′-H_{ax}, 6′′-H_{ax}, and 5′′-H_{ax}), 1.30 (1H, ddd, J=12.6, 4.4 Hz, 4′′-H_{ax}); ^{13}C NMR δ: 162.6 (d, $^1J_{C-F}$ = 246.4 Hz, 4'), 153.2 (*C*O), 141.2 (1), 138.6 (3), 136.9 (d, $^4J_{C-F}$ = 3.1 Hz, 1'), 129.5 (5), 128.7 (d, $^3J_{C-F}$ = 8.0 Hz, 2', 6'), 121.9 (6), 117.4 (d, $^2J_{C-F}$ = 21.5 Hz, 3', 5'), 115.7 (4), 115. 5 (2), 73.9 (1"), 32.0 (2′′,6′′), 25.4 (4′′), 23.8 (3′′, 5′′). Anal. Calcd. for $C_{20}H_{22}FNO_2$: C, 73.37; H, 6.77; N, 4.28. Found: C, 73.47; H, 6.72; N, 4.21.

*4.1.13.Benzyl (4'-fluoro-[1,1'-biphenyl]-3-yl)carbamate (**3b**).* The product, prepared starting from **4c** and phenyl methanol and purified by chromatography on silica gel (petroleum

ether:EtOAc, 85:15 v/v), was obtained as a white solid in 84% yield. mp 82.2-82.8 °C. TLC (petroleum ether: EtOAc, 80:20 v/v): Rf=0.55; IR (Nujol): 3278, 1696, 1612, 1554, 1512, 1494, 1241, 1218, 1102, 1077, 790 cm^{-1}; ^{1}H NMR ($CDCl_3$, 500 MHz) δ: 7.74 (1H, bs, 2-H), 7.58-7.53 (2H, AA′ part of AA′BB′ system, 2'- and 6'-H), 7.46-7.36 (6H, m, 5, 2′′, 3′′, 4′′, 5′′, 6′′-H), 7.33 (1H, ddd, J=7.8, <1.0, <1.0 Hz, 4-H), 7.27 (1H, ddd, J=7.8, <1.0, <1.0 Hz, 6-H), 6.79 (1H, bs, NH), 5.25 (2H, s, C*H*$_2$); ^{13}C NMR δ: 162.6 (d, $^{1}J_{C-F}$ = 246.5 Hz, 4'), 153.4 (*C*O), 141.3 (1), 138.3 (3), 136.9 (d, $^{4}J_{C-F}$ = 3.1 Hz, 1'), 136.0 (1"), 129.5 (5), 128.8 (d, $^{3}J_{C-F}$ = 8.0 Hz, 2', 6'), 128.7, 128.6, 128.5, 128.4 (1", 2′′, 3′′, 4′′, 5′′, 6′′), 122.3 (6), 117.4 (d, $^{2}J_{C-F}$ = 22.7 Hz, 3', 5'), 115.7 (4), 115.6 (2), 67.2 (*C*H$_2$). Anal. Calcd. for $C_{20}H_{16}FNO_2$: C, 74.75; H, 5.02; N, 4.36. Found: C, 74.77; H, 5.14; N, 4.56.

*4.1.14. Synthesis of 1,3-di([1,1'-biphenyl]-3-yl)urea (**5**).* CDI (115 mg, 7.08 mmol, 4 eq.), and **4a** (300 mg, 1.77 mmol, 1 eq.) were mixed in dry toluene (8 ml) and heated at reflux for 12 h under nitrogen atmosphere. After cooling to room temperature white precipitates were collected by filtration, washed with diethyl ether and cold CH_2Cl_2/ CH_3CN to obtain 255 mg (0.70 mmol, 89%) of **2** as a white crystalline solid. mp 258.2-259.0 °C; TLC (petroleum ether: EtOAc, 90:10 v/v): Rf=0.24; IR (Nujol): 3300, 1635, 1601, 1555, 1497, 1398, 1271, 1075, 785, 698 cm^{-1}; ^{1}H NMR (*d*$_6$-DMSO) δ: 8.85 (2H, s, 2 x NH), 7.83 (2H, dd, J=1.9, 1.9 Hz, 2 x 2-H), 7.63 (4H, dd, J=7.7, 1.0 Hz, 2 x 2'- and 6'-H), 7.48 (4H, dd, J=7.7, 7.7 Hz, 2 x 3'- and 5'-H), 7.42 (2H, ddd, J=8.1, 1.9, 1.2 Hz, 2 x 4-H), 7.40-7.35 (4H, m, 2 x 5- and 4'-H), 7.27 (2H, ddd, J=8.1, 1.9, 1.2 Hz, 2 x 6-H). ^{13}C NMR δ: 153.2 (*C*O), 141.3 (1'), 140.8 (1), 140.7 (3), 129.8 (5), 129.4 (3', 5'), 128.0 (4'), 127.1 (2', 6'), 120.8 (6), 117.9 (4), 117.0 (2). Anal. Calcd. for $C_{25}H_{20}N_2O$: C, 82.39; H, 5.53; N, 7.69. Found: C, 82.42; H, 5.68; N, 7.52.

4.2. Biological Section.

4.2.1. Enzyme kinetics study on human recombinant MAGL (hMAGL). For kinetic experiments, the assay was performed in a 96-well black plate in a total volume of 100 µl per well. The reaction mixture consisted of 25 ng/well of hMAGL and 5 µM (final concentration) of 7-HRA substrate (prepared in DMSO) in assay buffer solution consisting of 50 mM Tris-HCl (pH 7.4, 1 mM EDTA) and 10% DMSO (final concentration) at room temperature.

For hMAGL inhibitors testing, 25 ng/well of hMAGL dissolved in assay buffer (50mM Tris-HCl pH 7.4, 1 mM EDTA) are added to 80 µl of buffer solution; 5 µl of inhibitor solution in DMSO (between 10 to 75 µM) or DMSO alone were added and then incubated at room

temperature for 60 minutes. After incubation, the reaction was started by the rapid addition of 5 µl of 7-HRA intermediate solution to obtain the final concentration of 5 µM in the final volume of 100 µl. The fluorescence was measured at different time by Promega-GloMax multidetection system and the fluorescence unit converted to amount of resorufin produced (λex = 571 nm, λem = 588 nm) basing on a calibration curve by using standard solutions in DMSO (10 µl of standard in 90 µl of buffer).

In the kinetic study, different concentrations of hMAGL and 7-HRA were tested and no inhibitor solutions were added.

The reaction rate was determined by linear regression analyses ($r^2 \geq 0.98$) of the fluorescence emission increase over time. The background reaction rate with no enzyme present was subtracted and the reaction rates were normalized to the reaction rate with no inhibitor present (100%).

The IC_{50} values were calculated after 30 minutes and derived from two independent experiments performed in triplicate, calculated as nonlinear regressions using sigmoid dose–response setting with variable Hill slope by GraphPad Prism 5.0 for Windows.

*4.2.2. Inhibitor selectivity of compounds **2b** and **2c** with hFAAH.* For selectivity tests, in a 96 well black plate to each well, containing 184.5 µl of reaction buffer (50 mM TRIS-HCl, 1mM EDTA, pH 9), were added 1U of hFAAH and 2 µl of **2b** or **2c** or OEtA (1mM in DMSO) to reach a final concentration of 10 µM. After 1h of incubation at room temperature was added 1 µl of AAMCA (2mM in DMSO) to reach final concentration of 20 µM. The reaction was run for 30 minute in a JASCO fluorimeter with fluorescence readings taken every 3 minutes at a wavelength of 460 nm applying an excitation wavelength of 360 nm. As done for MAGL the reaction rate was determined by linear regression analyses ($r^2 \geq 0.98$) of the fluorescence emission increase over time. The background reaction rate with no enzyme present was subtracted and the reaction rates were normalized to the reaction rate with no inhibitor present (100%) (Supplementary fig. S4).

4.2.3. Cell lines and culture techniques. B16-F10, B16-F1 melanoma cell lines, MCF7 adenocarcinoma and HEK293T embryonic kidney cell lines were obtained from American Type Culture Collection (Rockville, Md., USA). Melanoma cells were cultured in Iscoves's medium supplemented with 10% heat-inactivated (56 °C) fetal bovine serum (FBS), 2 mM L-glutamine, 100 IU/ml penicillin G sodium, 100 lg/ml streptomycin sulfate (Euroclone, Milan,

Italy). MCF7 were cultured in 50% Dulbecco's modified Eagle's medium (DMEM) high glucose and 50% Ham's F-12 nutrient mixture, supplemented 10% heat-inactivated (56 °C) fetal bovine serum (FBS), 2 mM L-glutamine, 100 IU/ml penicillin G sodium, 100 lg/ml streptomycin sulfate. HEK293T were cultured in 50% Dulbecco's modified Eagle's medium (DMEM) high glucose supplemented 10% heat-inactivated (56 °C) fetal bovine serum (FBS), 2 mM L-glutamine, 100 IU/ml penicillin G sodium, 100 lg/ml streptomycin sulfate. Cells were maintained in a humidified atmosphere of 5% CO_2 in air at 37 °C.

4.2.4. Enzyme kinetic study on cancer cell lysates and intact cells. B16-F10 melanoma cells,[19,28] after 36 h of culture, were homogenised for 30 min at 4° C in lysis buffer (10 mM Tris, 150 mM NaCl, 1 mM EDTA, 0.1% SDS, 1% Triton X-100 with protease inhibitor mixture, pH 7.4) and lysates were then centrifuged for 5 min at 1,500 × g.
The assay was carried out in a 96-well format using 1 μg of cell lysate and 10 μM of substrate. To test the inhibitors, B16-F10 melanoma cells lysate was pre-treated for 60 min with DMSO or the compounds at different concentrations. Then, the substrate was added to each well and fluorescence was measured every 2.5 min for 2 h at 588 nm (λex.571 nm/λem.588 nm) by a Glomax-Microplate Multimode Reader (Promega). The graphs show the results after 5 min of incubation. Values are expressed as mean ± SEM (n = 3).
For the evaluation of MAGL activity in intact cells, B16-F10 melanoma cells were cultured in presence of compounds **2b-c** or DMSO for 6 h and then homogenised for 30 min at 4° C in lysis buffer. Lysates were then centrifuged for 5 min at 1,500 × g and the assay was carried out as described above using 1 μg of cell lysate and 10 μM of substrate. The graphs show the results after 5 min of incubation. Values are expressed as mean ± SEM (n = 3).

4.2.5. Proliferation assay. B16-F10 cell proliferation was assessed by measuring the cell divisions by flow cytometry.[30] Cells were stained by the CytoTrack Cell Proliferation Assays (CytoTrack Red 628/643; Bio-Rad, Hercules, CA, USA), according to the manufacturer's protocol and analysed by Gallios Flow Cytometer (Beckman-Coulter, Brea, CA, USA). The proliferation index, i.e. the average number of cells that an initial cell became, was calculated using the FCS Express 4 software (De Novo System, Portland, OR, USA).

4.2.6. Apoptosis assay. Cell death was evaluated by annexin V/propidium iodide (PI) staining via flow cytometry.[30,40] Briefly, cells were incubated with Alexa Fluor® 488 annexin V (ThermoFisher Scientific, Waltham, MA, USA) (5 μl x 10^6 cells) to assess the

phosphatidylserine exposure on the cell surface, and 5 μg/ml PI to exclude necrotic cells in binding buffer (10 mM HEPES, 140 mM NaCl, 2.5 mM CaCl2). Annexin V (FL-1) and PI (FL-3) fluorescences were measured in 10,000 cells per sample by Gallios Flow Cytometer.

4.2.7. Real-time PCR. The analysis of mRNA expression was performed as previously described.[30,40] Briefly, total RNA from B16-F10, B16-F10, MCF7 and HEK293T cells was extracted with the Purezol RNA Isolation Kit (Bio-rad), according to the manufacturer's protocol. First-strand cDNA was generated from 1 μg of total RNA using iScript Reverse Transcription Supermix (Bio-Rad). A set of primer pairs was designed to hybridize to unique regions of the appropriate gene sequence (Supplementary Table S1). PCR was performed using SsoAdvanced Universal SYBR Green Supermix and the CFX96 Touch Real-Time PCR Detection System (Bio-Rad). The fold change was determined relative to the control after normalizing to β-actin (internal standard) through the use of the formula 2-ΔΔCT.

4.3. Molecular Modelling.

4.3.1. In silico molecular docking simulations. Molecular docking of all the investigated compounds has been carried out on a crystallographic hMAGL 3D structure obtained from RCSB PDB, code 3JW8,[23] while hMAGL 3D structure obtained from RCSB PDB, code 3JWE[23] was used for the binding studies of the activator compound **5**. The protein was prepared through the Structure Preparation program of the Molecular Operating Environment (MOE) Prepare module [https://www.chemcomp.com/MOE-Mocular_Operating_Environment. htm]. This tool is useful for checking and correcting structures and preparing macromolecular data for further computational analysis.

A database, containing target compounds, was manually built by the MOE Builder program. All the compounds were energy minimized by the Energy Minimize program with default parameters of the MOE Compute module, to produce a single low-energy conformation for each putative ligand.

The enzyme binding site was identified by the use of the MOE Site Finder program, which uses a geometric approach to calculate possible binding sites in a receptor starting from its 3D atomic coordinates. This method is based not on energy models but on alpha spheres, which are a generalization of convex hulls.

The *in silico* screening was carried out with the MOE Dock program contained in the Compute module. The full MAGL structure was set as receptor and the binding site was delimited by a set of dummy atoms previously defined by the Site Finder analysis.

Before starting with the placement procedure, conformations were generated for each ligand by sampling their rotatable bonds. The selected placement methodology was Triangle Matcher, in which the poses are generated by superposing triplets of ligand atoms and triplets of receptor site points. The receptor site points are alpha spheres centers that represent locations of tight packing. Before scoring all the generated poses, duplicate complexes were removed. Poses are considered as duplicates if the same set of ligand-receptor atom pairs are involved in hydrogen bond interactions and the same set of ligand atom receptor residue pairs are involved in hydrophobic interactions. The accepted poses were scored according to the London dG scoring, which estimates the free energy of binding of the ligand from a given pose. The top-scoring 30 poses were passed to a refinement step based on molecular mechanics and then rescored according to the GBVI/WSA dG, a forcefield-based scoring function that estimates the free energy of binding of the ligand from a given pose. It has been trained using the MMFF94x and Amber99 force field on the 99 protein–ligand complexes of the SIE training set.[41] In order to speed up the calculation, residues over a 6 Å cut-off distance away from the pre-refined pose were ignored, both during the refinement and in the final energy evaluation. All receptor atoms were held fixed during the refinement. By default, during the refinement, solvation effects are calculated using the reaction field functional form for the electrostatic energy term and a dielectric constant of 4 and the final energy is evaluated using the Generalized Born solvation model (GB/VI).

The estimated binding free energy (affinity) of the top-scoring solution (selected according to the docking score) for all the investigated compounds, the complexes were further refined through the use of a set of specific MOE procedures, named QuickPrep, aimed at the minimization of ligands in the receptor binding site. During molecular docking procedures, the MMFF94x force field was used both for protein and ligands. Dissociation constant (K_i) was computed through the following equation: $K_i = e^{\Delta G/RT}$, where R represents the gas constant and T the absolute temperature, set at 300 K.

4.3.2. Pharmacophoric model.

The pharmacophoric model was built by the MOE Pharmacophore Elucidator using default settings. The IC_{50} value of the inactive compound was defined as the cut-off for satisfying the pharmacophoric queries. The unified scheme was selected as set of rules for defining the available features. Only the top scoring poses from molecular docking were selected for building the model, after a refinement flexible alignment of the chemicals.

Statistical analysis. Data are expressed as mean ± S.E.M. of single determinations performed in three or four independent experiments at different days. IC_{50} values were calculated by nonlinear regression using sigmoid dose–response setting with variable Hill slope by GraphPad Prism 5.0 for Windows. A p value < 0.05 (*) was considered significant. For proliferation and apoptosis assays statistical significance of raw data between the groups in each experiment was evaluated using one-way ANOVA followed by the Tukey's post-test (multiple comparisons).

Acknowledgements
This work was supported by: "Università di Milano, Linea 2 – Azione A 2016-2017" funding to P.C., C.P. and I.E.; MIUR Progetto Eccellenza.

A. Supplementary data

References

1. Zechner R, Zimmermann R, Eichmann TO, Kohlwein SD, Haemmerle G, Lass A, Madeo F. Fat Signals - Lipases and Lipolysis in Lipid Metabolism and Signaling. *Cell Metab*. 2012;15(3):279-291. doi:10.1016/j.cmet.2011.12.018.
2. Karlsson M, Contreras JA, Hellman U, Tornqvist H, Holm C. cDNA Cloning, Tissue Distribution, and Identification of the Catalytic Triad of Monoglyceride Lipase: Evolutionary Relationship to Esterases, Lysophospholipases, and Haloperoxidases. *J Biol Chem*. 1997;272(43):27218-27223. doi:10.1074/jbc.272.43.27218.
3. Schlosburg JE, Blankman JL, Long JZ, Nomura DK, Pan B, Kinsey SG, Nguyen PT, Ramesh D, Booker L, Burston JJ, Thomas EA, Selley D E, Sim-Selley L J, Liu Q, Lichtman AH, Cravatt BF. Chronic monoacylglycerol lipase blockade causes functional antagonism of the endocannabinoid system. *Nat Neurosci*. 2010;13(9):1113-1119. doi:10.1038/nn.2616.
4. Chanda PK, Gao Y, Mark L, Btesh J, Strassle BW, Lu P, Piesla MJ, Zhang M-Y, Bingham B, Uveges A, Kowal D, Garbe D, Kouranova EV, Ring R H, Bates B, Pangalos MN, Kennedy JD, Whiteside GT, Samad TA. Monoacylglycerol Lipase Activity Is a Critical Modulator of the Tone and Integrity of the Endocannabinoid System. *Mol Pharmacol*. 2010;78(6):996-1003. doi:10.1124/mol.110.068304.
5. Savinainen JR, Saario SM, Laitinen JT. The serine hydrolases MAGL, ABHD6 and ABHD12 as guardians of 2-arachidonoylglycerol signalling through cannabinoid receptors. *Acta Physiol*. 2012;204(2):267-276. doi:10.1111/j.1748-1716.2011.02280.x.
6. Di Marzo V, Bisogno T, De Petrocellis L. Endocannabinoids and Related Compounds: Walking Back and Forth between Plant Natural Products and Animal Physiology. *Chem Biol*. 2007;14(7):741-756. doi:10.1016/j.chembiol.2007.05.014.
7. Long JZ, Li W, Booker L, Burston JJ, Kinsey SG, Schlosburg JE, Pavón FJ, Serrano AM, Selley DE, Parsons LH, Lichtman AH, Cravatt BF. Selective blockade of 2-arachidonoylglycerol hydrolysis produces cannabinoid behavioral effects. *Nat Chem*

Biol. 2009;5(1):37-44. doi:10.1038/nchembio.129.

8. Janero DR, Makriyannis A. Targeted modulators of the endogenous cannabinoid system: Future medications to treat addiction disorders and obesity. *Curr Psychiatry Rep*. 2007;9(5):365-373. doi:10.1007/s11920-007-0047-1.

9. Comelli F, Giagnoni G, Bettoni I, Colleoni M, Costa B. The inhibition of monoacylglycerol lipase by URB602 showed an anti-inflammatory and anti-nociceptive effect in a murine model of acute inflammation. *Br J Pharmacol*. 2007;152(5):787-794. doi:10.1038/sj.bjp.0707425.

10. Hohmann AG. Inhibitors of monoacylglycerol lipase as novel analgesics. *Br J Pharmacol*. 2007;150(6):673-675. doi:10.1038/sj.bjp.0707153.

11. Nomura DK, Morrison BE, Blankman JL, Long JZ, Kinsey SG, Marcondes MCG, Ward AM, Hahn YK, Lichtman AH, Conti B, Cravatt BF. Endocannabinoid Hydrolysis Generates Brain Prostaglandins That Promote Neuroinflammation. *Science*. 2011;334(6057):809-813. doi:10.1126/science.1209200.

12. Wiskerke J, Irimia C, Cravatt BF, De Vries TJ, Schoffelmeer ANM, Pattij T, Parsons LH. Characterization of the Effects of Reuptake and Hydrolysis Inhibition on Interstitial Endocannabinoid Levels in the Brain: An in Vivo Microdialysis Study. *ACS Chem Neurosci*. 2012;3(5):407-417. doi:10.1021/cn300036b.

13. Taschler U, Radner FPW, Heier C, Schreiber R, Schweiger M, Schoiswohl G, Preiss-Landl K, Jaeger D, Reiter B, Koefeler HC, Wojciechowski J, Theussl C, Penninger JM, Lass A, Haemmerle G, Zechner R, Zimmermann R. Monoglyceride Lipase Deficiency in Mice Impairs Lipolysis and Attenuates Diet-induced Insulin Resistance. *J Biol Chem*. 2011;286(20):17467-17477. doi:10.1074/jbc.M110.215434.

14. Saario SM, Laitinen JT. Therapeutic Potential of Endocannabinoid-Hydrolysing Enzyme Inhibitors. *Basic Clin Pharmacol Toxicol*. 2007;101(5):287-293. doi:10.1111/j.1742-7843.2007.00130.x.

15. Qin H, Ruan Z. The Role of Monoacylglycerol Lipase (MAGL) in the Cancer Progress. *Cell Biochem Biophys*. 2014;70(1):33-36. doi:10.1007/s12013-014-9899-2.

16. Labar G, Bauvois C, Borel F, Ferrer J-L, Wouters J, Lambert DM. Crystal Structure of the Human Monoacylglycerol Lipase, a Key Actor in Endocannabinoid Signaling. *ChemBioChem*. 2010;11(2):218-227. doi:10.1002/cbic.200900621.

17. Tarzia G, Duranti A, Tontini A, Piersanti G, Mor M, Rivara S, Plazzi PV, Park C, Kathuria S, Piomelli DJ. Design, Synthesis, and Structure−Activity Relationships of Alkylcarbamic Acid Aryl Esters, a New Class of Fatty Acid Amide Hydrolase Inhibitors. *J Med Chem*. 2003;46(12):2352-2360. doi:10.1021/jm021119g.

18. Long JZ, Nomura DK, Cravatt BF. Characterization of Monoacylglycerol Lipase Inhibition Reveals Differences in Central and Peripheral Endocannabinoid Metabolism. *Chem Biol*. 2009;16(7):744-753. doi:10.1016/j.chembiol.2009.05.009.

19. Aaltonen N, Savinainen JR, Ribas CR, Rönkkö J, Kuusisto A, Korhonen J Navia-Paldanius D, Hayrinen J, Takabe P, Kasnanen H, Pantsar T, Laitinen T, Lehtonen M, Pasonen-Seppanen S, Poso A, Nevalainen T, Laitinen JT. Piperazine and Piperidine Triazole Ureas as Ultrapotent and Highly Selective Inhibitors of Monoacylglycerol Lipase. *Chem Biol*. 2013;20(3):379-390. doi:10.1016/j.chembiol.2013.01.012.

20. Makara JK, Mor M, Fegley D, Szabó SI, Kathuria S, Astarita G, Duranti A, Tontini A, Tarzia G, Rivara S, Freund TF, Piomelli D. Selective inhibition of 2-AG hydrolysis enhances endocannabinoid signaling in hippocampus. *Nat Neurosci*. 2005;8(9):1139-1141. doi:10.1038/nn1521.

21. Szabo M, Agostino M, Malone DT, Yuriev E, Capuano B. The design, synthesis and biological evaluation of novel URB602 analogues as potential monoacylglycerol lipase inhibitors. *Bioorg Med Chem Lett*. 2011;21(22):6782-6787. doi:10.1016/j.bmcl.2011.09.038.

22. Pagano E, Borrelli F, Orlando P, Romano B, Monti M, Morbidelli L, Aviello G, Imperatore R, Capasso R, Piscitelli F, Buono L, Di Marzo V, Izzo AA. Pharmacological inhibition of MAGL attenuates experimental colon carcinogenesis. *Pharmacol Res*. 2017;119:227-236. doi:10.1016/j.phrs.2017.02.002.

23. Bertrand T, Augé F, Houtmann J, Rak A, Vallée F, Mikol V, Berne PF, Michot N, Cheuret D, Hoornaert C, Mathieu MJ. Structural Basis for Human Monoglyceride Lipase Inhibition. *J Mol Biol*. 2010;396(3):663-673. doi:10.1016/j.jmb.2009.11.060.

24. Nomura DK, Long JZ, Niessen S, Hoover HS, Ng S-W, Cravatt BF. Monoacylglycerol Lipase Regulates a Fatty Acid Network that Promotes Cancer Pathogenesis. *Cell*. 2010;140(1):49-61. doi:10.1016/j.cell.2009.11.027.

25. Padiya KJ, Gavade S, Kardile B, Tiwari M, Bajare S, Mane M, Gaware V, Varghese S, Harel D, Kurhade S. Unprecedented "In Water" Imidazole Carbonylation: Paradigm Shift for Preparation of Urea and Carbamate. *Org Lett*. 2012;14(11):2814-2817. doi:10.1021/ol301009d.

26. Lauria S, Casati S, Ciuffreda P. Synthesis and characterization of a new fluorogenic substrate for monoacylglycerol lipase and application to inhibition studies. *Anal Bioanal Chem*. 2015;407(26). doi:10.1007/s00216-015-8991-9.

27. Wang Y, Chanda P, Jones PG, Kennedy JD. A Fluorescence-Based Assay for Monoacylglycerol Lipase Compatible with Inhibitor Screening. *Assay Drug Dev Technol*. 2008;6(3):387-393. doi:10.1089/adt.2007.122.

28. Hamtiaux L, Masquelier J, Muccioli GG, Bouzin C, Feron O, Gallez B, Lambert DM. The association of N-palmitoylethanolamine with the FAAH inhibitor URB597 impairs melanoma growth through a supra-additive action. *BMC Cancer*. 2012;12(1):92. doi:10.1186/1471-2407-12-92.

29. King AR, Duranti A, Tontini A, Rivara S, Rosengarth A, Clapper JR, Astarita G, Geaga JA, Luecke H, Mor M, Tarzia G, Piomelli D. URB602 Inhibits Monoacylglycerol Lipase and Selectively Blocks 2-Arachidonoylglycerol Degradation in Intact Brain Slices. *Chem Biol*. 2007;14(12):1357-1365. doi:10.1016/j.chembiol.2007.10.017.

30. Perrotta C, Buonanno F, Zecchini S, Giavazzi A, Proietti Serafini F, Catalani E, Guerra L, Belardinelli MC, Picchietti S, Fausto AM, Giorgi S, Marcantoni E, Clementi E, Ortenzi C, Cervia D. Climacostol reduces tumour progression in a mouse model of melanoma via the p53-dependent intrinsic apoptotic programme. *Sci Rep*. 2016;6:27281. doi:10.1038/srep27281.

31. Li F, Fei X, Xu J, Ji C. An unannotated α/β hydrolase superfamily member, ABHD6

differentially expressed among cancer cell lines. *Mol Biol Rep*. 2009;36(4):691-696. doi:10.1007/s11033-008-9230-7.

32. Max D, Hesse M, Volkmer I, Staege MS. High expression of the evolutionarily conserved α/β hydrolase domain containing 6 (ABHD6) in Ewing tumors. *Cancer Sci*. 2009;100(12):2383-2389. doi:10.1111/j.1349-7006.2009.01347.x.

33. Janicke RU. Caspase-3 Is Required for DNA Fragmentation and Morphological Changes Associated with Apoptosis. *J Biol Chem*. 1998;273(16):9357-9360. doi:10.1074/jbc.273.16.9357.

34. Vago R, Bettiga A, Salonia A, Ciuffreda P, Ottria R. Development of new inhibitors for N-acylethanolamine-hydrolyzing acid amidase as promising tool against bladder cancer. *Bioorg Med Chem*. 2017;25(3):1242-1249. doi:10.1016/j.bmc.2016.12.042.

35. Ramarao MK, Murphy EA, Shen MWH, Wang Y, Bushell KN, Huang N, Pan N, Williams C, Clark JD. A fluorescence-based assay for fatty acid amide hydrolase compatible with high-throughput screening. *Anal Biochem*. 2005;343(1):143-151. doi:10.1016/j.ab.2005.04.032.

36. Vandevoorde S, Jonsson K-O, Labar G, Persson E, Lambert DM, Fowler CJ. Lack of selectivity of URB602 for 2-oleoylglycerol compared to anandamide hydrolysis in vitro. *Br J Pharmacol*. 2007;150(2):186-191. doi:10.1038/sj.bjp.0706971.

37. Chen L, Lang H, Fang L, Zhu M, Liu J, Yu J, Wang L. Nickel-Catalyzed One-Pot Suzuki–Miyaura Cross-Coupling of Phenols and Arylboronic Acids Mediated by N,N-Ditosylaniline. *European J Org Chem*. 2014;2014(23):4953-4957. doi:10.1002/ejoc.201402475.

38. Hong WP, Iosub A V., Stahl SS. Pd-Catalyzed Semmler–Wolff Reactions for the Conversion of Substituted Cyclohexenone Oximes to Primary Anilines. *J Am Chem Soc*. 2013;135(37):13664-13667. doi:10.1021/ja4073172.

39. Hoggard LR, Zhang Y, Zhang M, Panic V, Wisniewski JA, Ji H. Rational Design of Selective Small-Molecule Inhibitors for β-Catenin/B-Cell Lymphoma 9 Protein–Protein Interactions. *J Am Chem Soc*. 2015;137(38):12249-12260. doi:10.1021/jacs.5b04988.

40. Cervia D, Assi E, De Palma C, Giovarelli M, Bizzozero L, Pambianco S, Di Renzo I, Zecchini S, Moscheni C, Vantaggiato C, Procacci P, Clementi E, Perrotta C. Essential role for acid sphingomyelinase-inhibited autophagy in melanoma response to cisplatin. *Oncotarget*. 2016;7(18):24995-25009. doi:10.18632/oncotarget.8735.

41. Naïm M, Bhat S, Rankin KN, Dennis S, Chowdhury SF, Siddiqi I, Drabik P, Sulea T, Bayly CI, Jakalian A, Purisima EO. Solvated Interaction Energy (SIE) for Scoring Protein−Ligand Binding Affinities. 1. Exploring the Parameter Space. *J Chem Inf Model*. 2007;47(1):122-133. doi:10.1021/ci600406v.

Table 1. Chemical structures, calculated partition coefficient (log P), dissociation constant values, and inhibitory activity of compounds **1a-c**, **2a-c**, **3a-b**, **5**.

	LogP[a]	*In silico*	*In vitro*	*Cell based assay*
Compound		Ki[b]	IC_{50}[c] (µM)	IC_{50}[c] (µM)
URB602	5.32	8.9e-06	9.1 ± 0.8[d]	19.79 ± 0.079
1a	4.69	7.4e-06	11.1 ± 2.3	16.48 ± 0.096
1b	5.44	6.0e-06	11.3 ± 1.4	17.14 ± 0.083
1c	4.27	1.3e-05	n.a.	n.a.
2a	6.22	1.6e-05	10.5 ± 2.0	17.40 ± 0.102
2b	5.91	3.0e-06	4.5 ± 0.7	9.414 ± 0.04
2c	5.16	3.3e-06	6.7 ± 0.7	13.19 ± 0.038
3a	5.49	7.7e-06	13.4 ± 0.9	26.69 ± 0.147
3b	5.17	4.8e-06	7.9 ± 0.8	15.61 ± 0.161
		Ki[b]	EC_{50}[e] (µM)	EC_{50}[e] (µM)
5	6.68	2.73e-06	2.8 ± 0.6[e]	5.76 ± 0.02[e]

[a] Calcd. using the Molinspiration Property Engine 2016.10 Program software. [b]The dissociation constant (K_i) values were computed through the binding free energy, according to the following equation: $K_i = e^{\Delta G/RT}$, where *R* represents the gas constant and *T* the absolute temperature, set at 300 K. [c]IC_{50} values are the means of three separate determinations and were determined by more than five concentrations of each inhibitor. [d]The compound URB602 was used as a positive control in the fluorometric assay. [e]EC_{50} values are the means of three separate determinations and were determined by more than five concentrations of compound **5**. Statistical calculation of IC_{50} and EC_{50} values was performed on GraphPad Prism 5.02 (GraphPad Software, Inc.).

Fig. 1

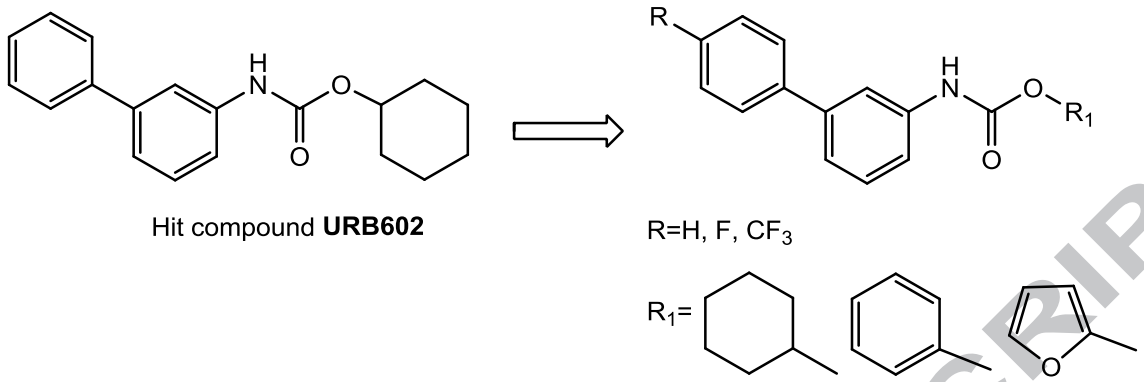

Scheme 1

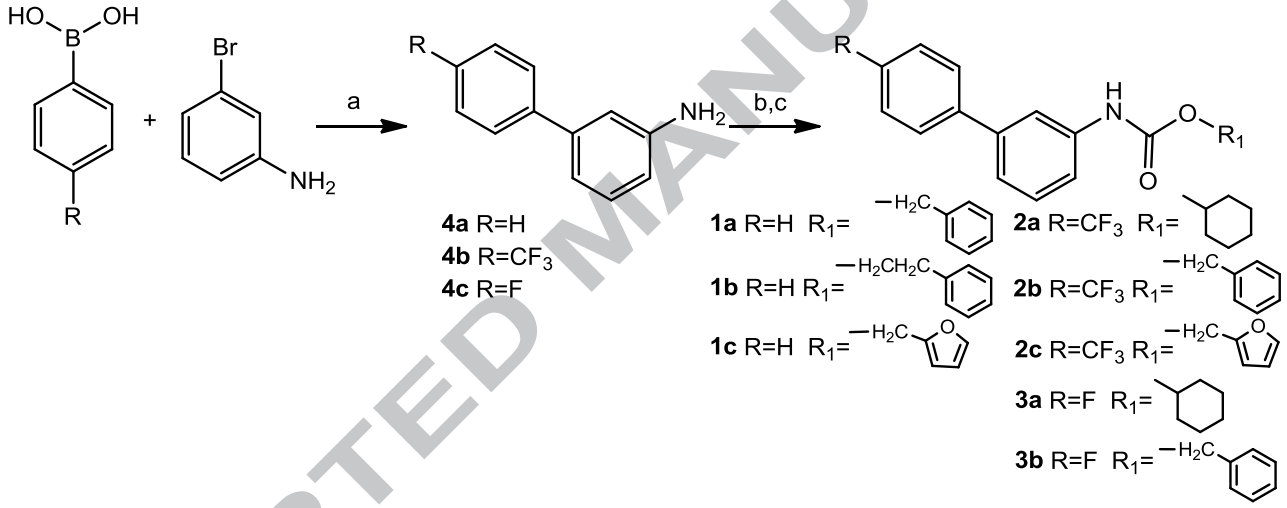

Scheme 2

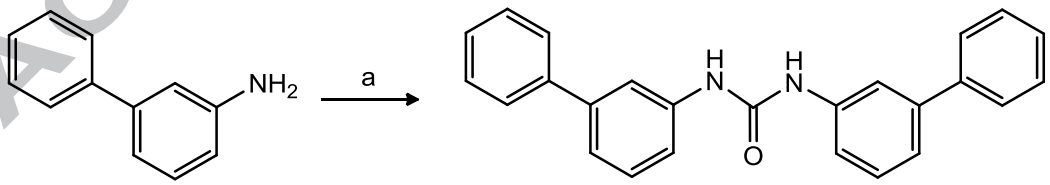

Fig. 2

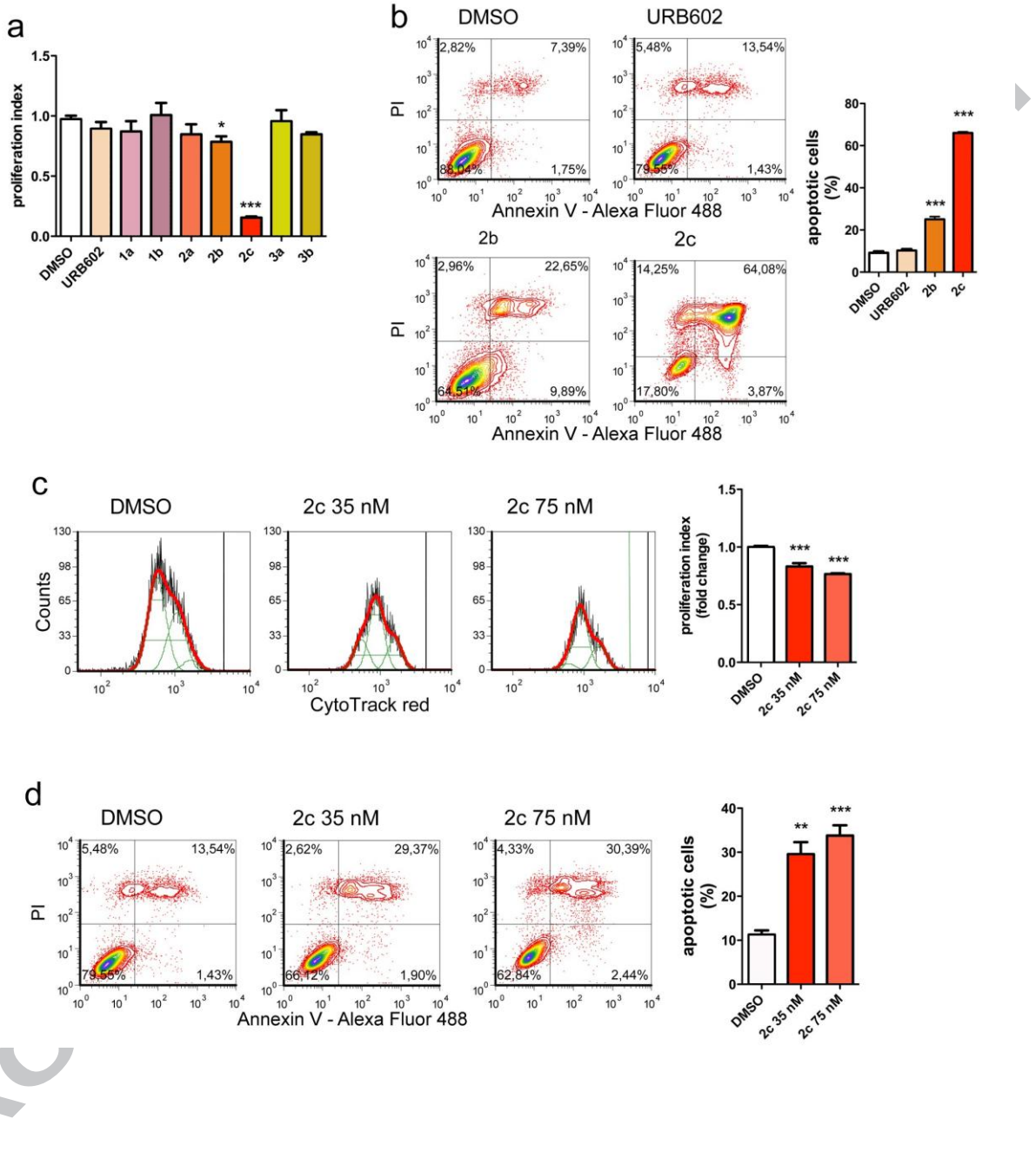

Fig. 3

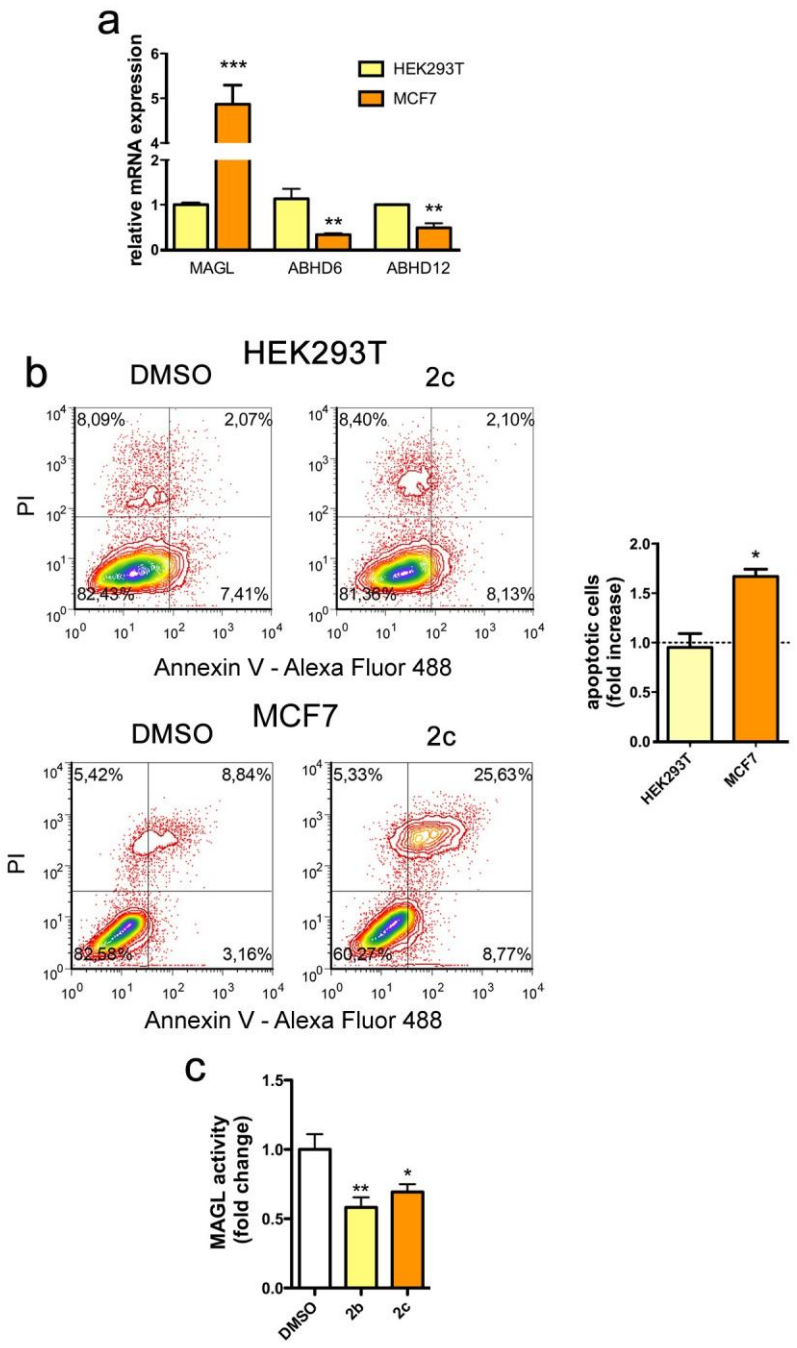
a
relative mRNA expression
HEK293T
MCF7
***
**
**
MAGL
ABHD6
ABHD12
b
HEK293T
DMSO
2c
8,09%
2,07%
82,43%
7,41%
8,40%
2,10%
81,36%
8,13%
PI
Annexin V - Alexa Fluor 488
MCF7
DMSO
2c
5,42%
8,84%
82,58%
3,16%
5,33%
25,63%
60,27%
8,77%
PI
Annexin V - Alexa Fluor 488
apoptotic cells (fold increase)
*
HEK293T
MCF7
c
MAGL activity (fold change)
**
*
DMSO
2b
2c

Fig. 4

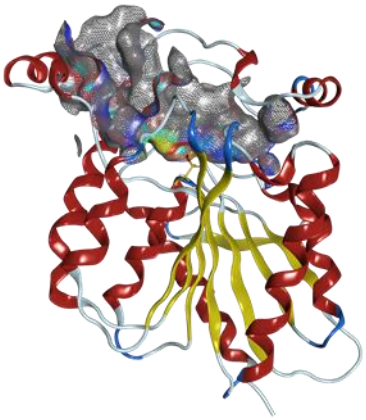

Fig. 5

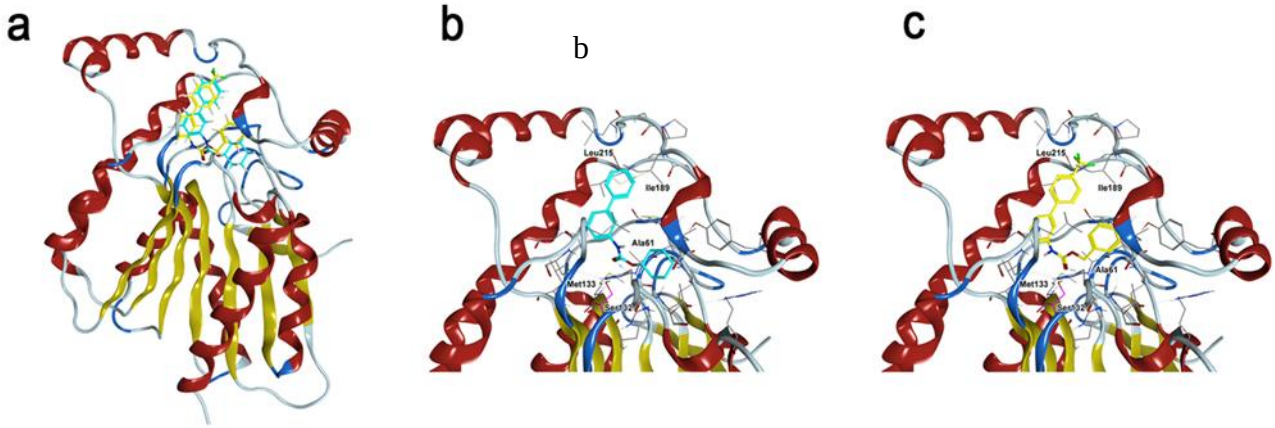

Fig. 6

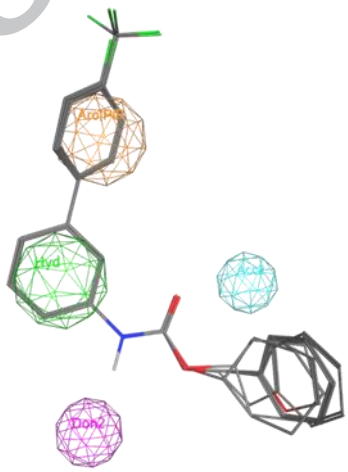

Fig. 7

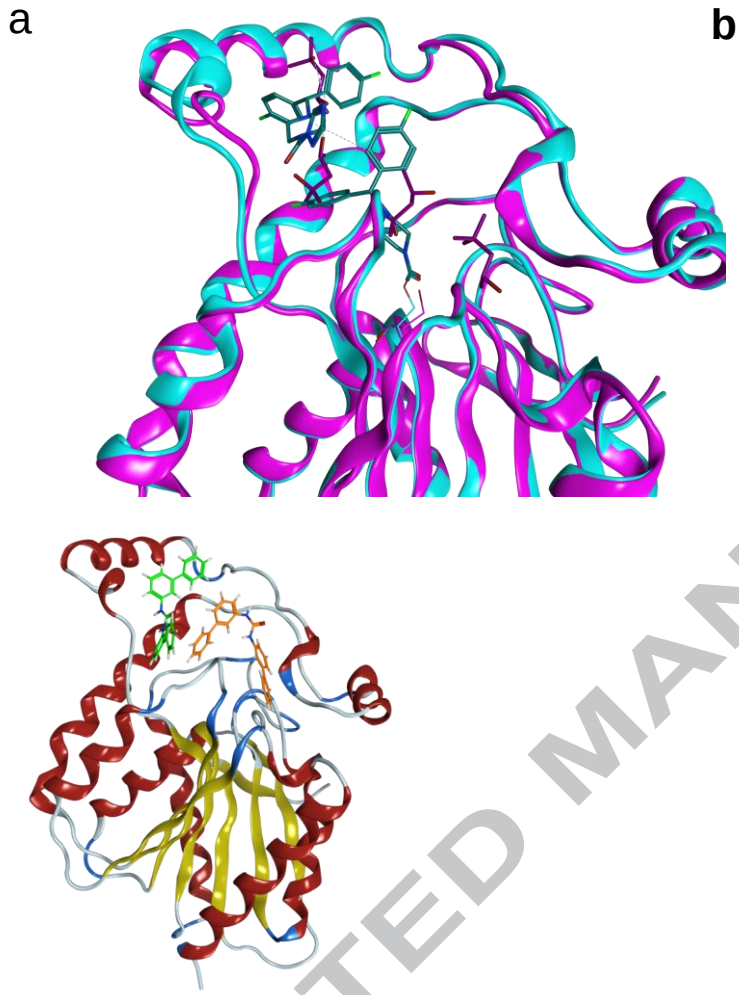

Fig. 8

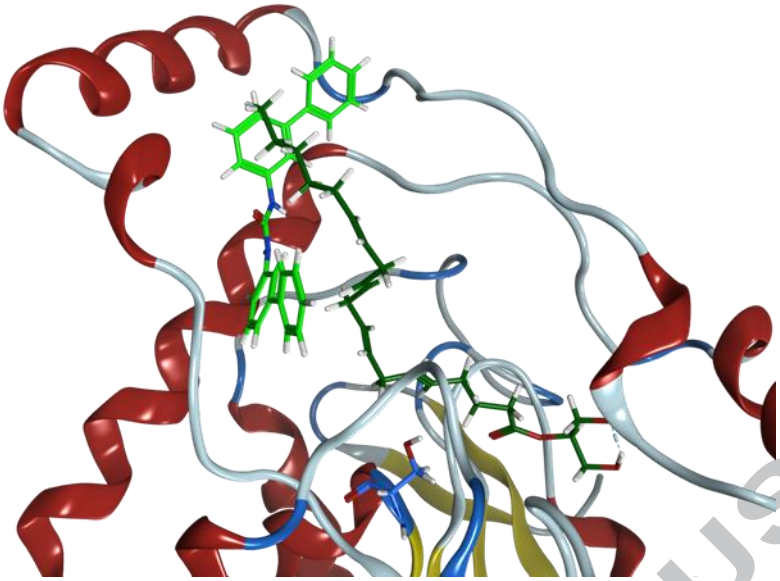

Captions

Scheme 1. Synthesis of compounds 1-2a-c 3a-b. Reagents and conditions: (a) $Pd(PPh_3)_4$, Na_2CO_3, CH_3OH, reflux, 12 h; (b) CDI, DMAP, CH_3CN, reflux, overnight; (c) R_1-OH, CH_3CN, reflux.

Scheme 2. Synthesis of compound 5. Reagents and conditions: (a) CDI, DMAP, CH_3CN, reflux, overnight.

Fig. 1. Structural modifications of hit compound URB602.

Fig. 2. Effect of synthetic compounds on cell proliferation and apoptosis. (a) B16-F10 cells were cultured in the presence of 10 μM of each compound for 48 h. Cell proliferation was analysed by flow cytometry. Data are expressed as the fold change of proliferation index over control (DMSO) (n = 3). *p < 0.05 and ***p < 0.0001 vs the respective control. (b) B16-F10 cells were treated with 10 μM of compounds **2b** and **2c** for 48 h. Cell death was analysed by flow cytometry. Images on the left are representative contour plots of Annexin V-FITC/PI staining. The graph on the right show the mean ± S.E.M. percentage of apoptotic cells (Annexin V^+/PI^- + Annexin V^+/PI^+ fraction; the Annexin V^-/PI^+ fraction, regarded as necrotic stage, was excluded) for 3 independent experiments. ***p < 0.0001 vs the respective control. (c, d) Evaluation of cell proliferation (c) and apoptosis (d) after treatment of cells with 35 nM and 75 nM of the compound **2c** for 48 h. Images on the left are representative proliferation (c) and contour plots (d). The vertical black line in the proliferation plots represents the undivided cell peak used as point of reference. Data in the graphs on the right are expressed as the fold change of proliferation index over control (DMSO treated cells) (c) and % of apoptotic cells (d) (n = 3). **p < 0.001 and ***p < 0.0001 vs the respective control.

Fig. 3. (a) evaluation of MAGL, ABHD6 and ABHD12 expression in MCF7 and HEK293T human cell lines. Data are expressed as fold change vs HEK293T (n=4). **p < 0.001; ***p < 0.0001 vs HEK293T. (b) Cell death analysis by flow cytometry. Right panel: representative contour plots of Annexin V-FITC/PI staining of HEK293T and MCF7 cells treated with 10 μM of compound **2c** for 48 h (n=3). The data in the graph are expressed as means ± S.E.M.. *p < 0.05 vs DMSO treated cells. (c) MCF7 cells were cultured for 6 h in the presence of the compounds 2b and 2c (10 μM). MAGL activity was measured on total cell lysate. *p < 0.05; **p < 0.001 vs DMSO treated cells.

Fig. 4. MAGL binding site according to the MOE Site Finder. 3JW8 is represented as ribbon and the binding site as a gray shaded molecular surface.

Fig. 5. Molecular recognition mechanism of MAGL inhibitors. (a) URB602 and compound **2b** docked to MAGL are represented in cyan and yellow stick, respectively. MAGL is represented as ribbon. (b) Detailed molecular interactions between MAGL residues and URB602 (b) and compound **2b** (c) in the catalytic pocket. Catalytic Ser132 is highlighted in magenta.

Fig. 6. Pharmacophoric model and structure activity relationship for MAGL inhibitors. The pharmacophore features are represented as colored spheres: orange for aromatic or Pi ring center, green for hydrophobic, cyan for H-bond acceptor and magenta for H-bond donor.

Fig. 7. MAGL binding site. (a) Focus on two different crystals of MAGL binding site: in magenta, crystal structure of 3JW8, with 4 co-crystallized MPD molecules; in light blue, crystal structure of 3JWE, with 2 co-crystallized SAR molecules. (b) Superposition of two activator::MAGL (3JWE) complexes: in orange, the activator in placed in the enzyme catalytic site; in green, the activator in the external binding site.

Fig. 8. MAGL can contemporarily bind out activator and a model substrate. Top scoring docking pose of 2-AG (dark green) with respect to the activator::MAGL complex (PDB: 3JWE) in the catalytic site. Ser132 of the catalytic triad is depicted in blue.

Graphical abstract

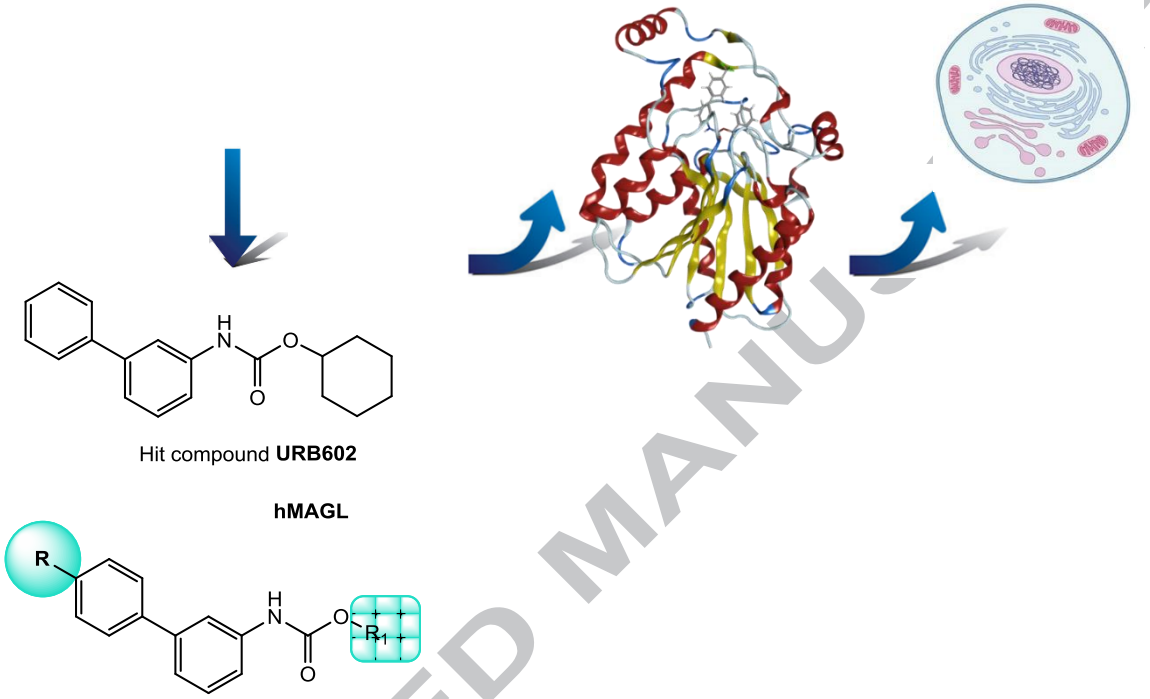

Research Highlights

Novel carbamate derivatives were synthesized and evaluated as hMAGL inhibitors.

Compound **2b** showed an IC_{50} as low as 4.5μM.
Structure-activity relationships were rationalized by the molecular modeling studies.

Studies in cancer cells confirmed MAGL inhibitory activity of compounds **2b** and **2c**.

Compounds **2b** and **2**c showed a higher anti-proliferative and cytotoxic activity.